Table 2
Number of hepatic miRNA whose expression changed at different times after HAL administration.

Time after administration (h)	Up-regulated (>two-fold)	Un-changed	Down-regulated (<0.5-fold)	Total
1	10	110	97	217
3	58	131	34	223
6	30	178	31	239
12	25	166	47	238
24	47	150	42	239

expression levels, we categorized these miRNAs into three groups as follows: an up-regulated (>two-fold) group, an unchanged (0.5- to 2-fold) group, and a down-regulated (<0.5-fold) group. The expression levels of approximately 30–50% of miRNAs changed more than two-fold at every time point.

A clustering analysis of the fold change in the miRNAs (Fig. 3) demonstrated that the profiles of the 1 h and 24 h group were classified the same group, while the profiles of the 3 h, 6 h and 12 h groups were classified other groups. Therefore, the time-dependent changes in the miRNA expression profile were not correlated with those of the ALT levels.

Because the miRNAs were differentially expressed in the liver at the beginning of the HAL-induced liver injury, we hypothesized that HAL affects the expression of miRNA, inducing the immune- and/or inflammation-related responses and therefore increasing the pro-inflammatory cytokine production that initiates liver injury. Therefore, to reveal the miRNA responsible for the early phase of HAL-induced liver injury, two time points (1 h and 3 h) after the administration were investigated further. In addition, to exclude any pharmacological effects on the miRNA expression profiles, we performed TaqMan microRNA array analysis of the hepatic miRNAs 1 h and 3 h after ISO administration. ISO is structurally and pharmacologically similar to HAL but is much less hepatotoxic (Njoku et al., 1997). The plasma ALT levels did not increase at 30 mmol/kg ISO. Over 200 miRNAs exhibited altered expression levels 1 or 3 h after ISO administration (Table 3). Histopathological study was conducted in the liver of ISO-administered mouse and no abnormalities were found (data not shown).

As presented in Fig. 4A, among the 10 up-regulated miRNAs in the 1 h after HAL-administered (1 h/HAL) group and the 49 up-regulated miRNAs in the 1 h after ISO-administered (1 h/ISO) group, 6 miRNAs were shared. Among the 97 down-regulated miRNAs in the 1 h/HAL group and the 43 down-regulated miRNAs in the 1 h/ISO group, 30 miRNAs were shared (Fig. 4A). Among the 58 up-regulated miRNAs in the 3 h/HAL group and the 64 up-regulated miRNAs in the 3 h/ISO group, 35 miRNAs were shared (Fig. 4B). Among the 34 down-regulated miRNAs in the 3 h/HAL group and the 32 down-regulated miRNAs in the 3 h/ISO group, 23 miRNAs were shared (Fig. 4B). We excluded the miRNAs whose expression was changed in both the HAL and ISO groups because they may be subject to pharmacological effects and therefore may not be associated with liver injury. Consequently, in subsequent studies, we focused on the miRNAs whose expressions were changed in the only HAL group.

To understand the purpose of miRNAs in biological processes and identify the pathogenetic pathways modified by posttranscriptional regulation, we performed an *in silico* pathway analysis for differentially expressed miRNAs in the HAL or ISO groups using DIANA-mirPath software (Vlachos et al., 2012). The DIANA-mirPath

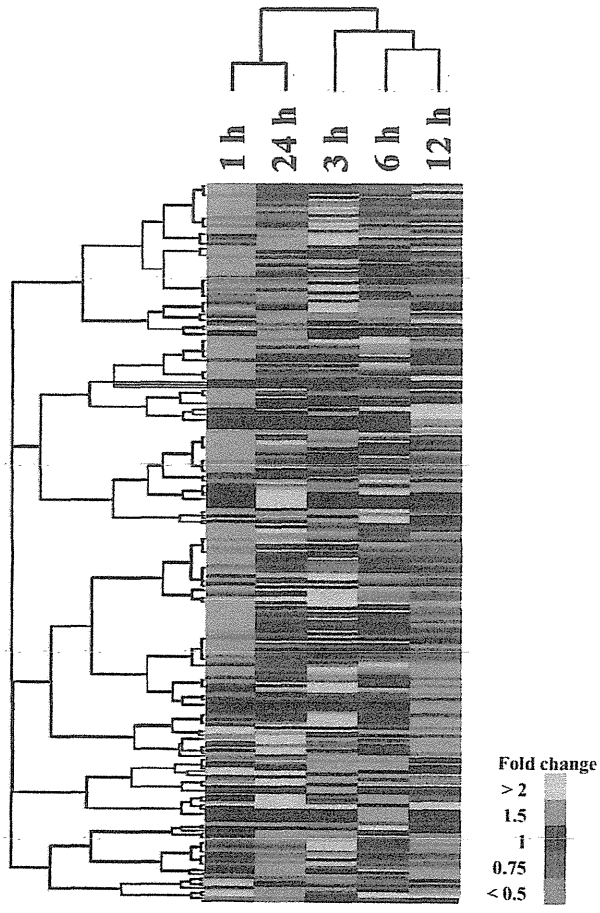

Fig. 3. Hierarchical clustering of the changes in the hepatic miRNA expression level between vehicle- or HAL-treated samples at five different intervals after HAL administration. The levels were clustered with Cluster 3.0 software (complete linkage) and visualized using MapleTree software.

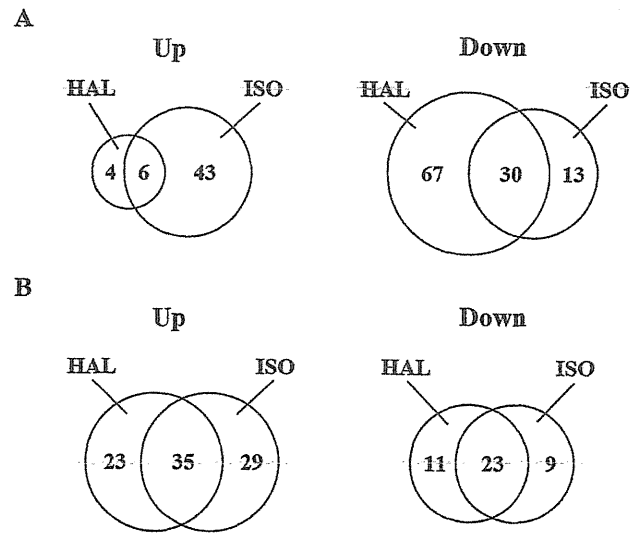

Fig. 4. Venn diagrams illustrating the overlap of miRNA changed at 1 h or 3 h after HAL or ISO administration. The up- and down-regulated miRNAs at least two-fold change in liver 1 h (A) and 3 h (B) after HAL and ISO administration, respectively. HAL: halothane-treated group, ISO: Isoflurane-treated group.

Table 3
Number of hepatic miRNA whose expression was changed shortly after ISO administration.

Time after administration (h)	Up (>two-fold)	Un-changed	Down (<0.5-fold)	Total
1	49	145	43	237
3	64	142	32	238

Table 4
List of enriched pathways ($P < 0.05$) in the genes predicted to be targeted by up-regulated microRNAs; these microRNAs exhibited at least a two-fold change in the liver values 1 h after HAL or ISO was administered.

HAL-administered group			ISO-administered group		
KEGG pathway	*P*-value	Number of genes	KEGG pathway	*P*-value	Number of genes
Pathways in cancer	0.03777	18	Pathways in cancer	9E−08	103
MAPK signaling pathway	0.02765	17	MAPK signaling pathway	0.0003	83
Bacterial invasion of epithelial cells	0.01574	7	Regulation of actin cytoskeleton	0.0003	72
mTOR signaling pathway	0.03777	5	Endocytosis	0.0016	67
Drug metabolism – cytochrome P450	0.00473	1	Focal adhesion	0.0023	63
			Wnt signaling pathway	4E−05	55
			Insulin signaling pathway	0.0003	50
			Tight junction	0.0095	43
			ErbB signaling pathway	2E−05	38
			Fc gamma R-mediated phagocytosis	0.0107	32
			mRNA surveillance pathway	0.0107	31
			Gap junction	0.0004	30
			TGF-beta signaling pathway	0.0034	28
			Adherens junction	0.0424	28
			Bacterial invasion of epithelial cells	0.0031	26
			Phosphatidylinositol signaling system	0.0226	26
			mTOR signaling pathway	0.0012	23
			Adipocytokine signaling pathway	0.0129	23
			Lysine degradation	3E−11	22
			Mucin type O-Glycan biosynthesis	1E−11	12
			Glycosaminoglycan biosynthesis – heparan sulfate	5E−26	10
			Glycosphingolipid biosynthesis – ganglio series	0.0343	5
			Glycosaminoglycan biosynthesis – chondroitin sulfate	0.0467	4

software executes an enrichment analysis of multiple miRNA target genes by comparing each set of miRNA targets to all known Kyoto Encyclopedia of Genes and Genomes (KEGG) pathways (Kanehisa, 2002; Kanehisa et al., 2006), this software is a valuable tool for elucidating targets that are affected by differentially altered miRNAs. During the *in silico* pathway analysis, the pathways regulated only in specific tissues, such as those in the brain or kidney, except for liver tissues were excluded.

Five and 23 targeted pathways from the 4 and 43 up-regulated miRNAs in 1 h/HAL and 1 h/ISO group, respectively, were predicted by the *in silico* analysis (Table 4). Forty-two and 8 pathways from the 67 and 13 down-regulated miRNAs in 1 h/HAL and 1 h/ISO group, respectively, were predicted (Table 5). The MAPK signaling pathway was shared among these putative targeted pathways for the 1 h group (Tables 4 and 5). The pathways related to inflammation, immune reactions and liver diseases, such as the Chemokine signaling pathway, the Jak-STAT signaling pathway, Hepatitis C, the T cell receptor signaling pathway, leukocyte transendothelial migration, and apoptosis were significantly enriched in the putative targeted pathways of the miRNA that was down-regulated in 1 h/HAL group but not the 1 h/ISO group (Table 5).

Twenty-eight and 29 pathways from the 23 and 29 up-regulated miRNAs in 3 h/HAL and 3 h/ISO group, respectively, were predicted (Supplemental Table 1). Ten and 16 pathways from the 11 and 9 down-regulated miRNAs in 3 h/HAL and 3 h/ISO group, respectively, were predicted (Supplemental Table 2). In both the 3 h/HAL and 3 h/ISO groups, similar pathways involved in inflammation, immune system and liver diseases such as MAPK signaling pathway, Cytokine/Chemokine-cytokine receptor interactions, the TGF-β signaling pathway, and the T cell receptor signaling pathway were significantly enriched.

Supplementary material related to this article can be found, in the online version, at http://dx.doi.org/10.1016/j.tox.2014.02.011.

Based on the KEGG pathway analyses, it was suggested that the miRNAs down-regulated 1 h after HAL administration are most likely involved in inflammation and immune system regulation, leading to the liver injury. Some pathways related to inflammation,

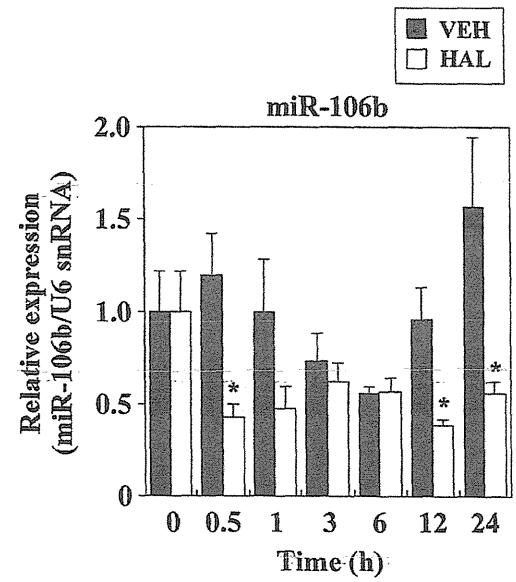

Fig. 5. Time-dependent changes in the hepatic miR-106b expression levels in HAL-induced liver injury. Mice were administered intraperitoneally with 30 mmol/kg HAL. At 0, 0.5, 1, 3, 6, 12 and 24 h after administration, the livers were collected to assess the hepatic miR-106b or U6 snRNA expression levels. Expression of hepatic miRNA was normalized to U6 snRNA. Data are represented as the means ± SEM ($n = 4$). *$P < 0.05$, compared to the VEH group at each time point. VEH: vehicle-treated group, HAL: halothane-treated group.

Table 5
List of enriched pathways ($P < 0.05$) in the genes predicted to be targets by down-regulated microRNAs; these microRNAs exhibited at least a two-fold change in the liver values 1 h after HAL or ISO was administered.

HAL-administered group			ISO-administered group		
KEGG pathway	*P*-value	Number of genes	KEGG pathway	*P*-value	Number of genes
Pathways in cancer	2.26E−08	145	Pathways in cancer	0.0012	26
MAPK signaling pathway	3.01E−07	122	MAPK signaling pathway	0.033	21
Focal adhesion	1.87E−09	105	Gap junction	5E−08	11
Regulation of actin cytoskeleton	2.74E−07	103	ErbB signaling pathway	0.0012	11
Endocytosis	0.00016	89	Lysine degradation	9E−07	7
Chemokine signaling pathway	0.013	73	Adherens junction	0.0146	5
Wnt signaling pathway	0.0019	68	Glycosphingolipid biosynthesis – lacto and neolacto series	6E−07	4
Insulin signaling pathway	0.00015	65	Glycosaminoglycan biosynthesis – keratan sulfate	0.0044	2
Protein processing in endoplasmic reticulum	0.03116	63			
Ubiquitin mediated proteolysis	0.00349	62			
Jak-STAT signaling pathway	0.01274	62			
Hepatitis C	0.03189	55			
T cell receptor signaling pathway	0.00108	53			
ErbB signaling pathway	2.19E−05	48			
Amoebiasis	0.00108	48			
Leukocyte transendothelial migration	0.0091	48			
Toxoplasmosis	0.03189	46			
Chagas disease (American trypanosomiasis)	0.01197	45			
Glycerophospholipid metabolism	0.00052	41			
Fc gamma R-mediated phagocytosis	0.00553	41			
Phosphatidylinositol signaling system	0.013	38			
ECM-receptor interaction	1.36E−06	36			
Gap junction	0.00047	36			
VEGF signaling pathway	0.00445	36			
Apoptosis	0.02019	36			
Fc epsilon RI signaling pathway	0.03805	35			
p53 signaling pathway	0.00142	34			
Bacterial invasion of epithelial cells	0.00532	33			
B cell receptor signaling pathway	0.03707	33			
mTOR signaling pathway	0.00173	29			
Hedgehog signaling pathway	0.00895	26			
Lysine degradation	3.57E−06	23			
SNARE interactions in vesicular transport	0.0017	18			
Sphingolipid metabolism	0.01294	18			
Fatty acid metabolism	0.04022	14			
Mucin type O-Glycan biosynthesis	2.75E−06	12			
Glycosphingolipid biosynthesis – lacto and neolacto series	1.63E−05	12			
Glycosaminoglycan biosynthesis – heparan sulfate	0.0001	11			
Glycosaminoglycan biosynthesis – chondroitin sulfate	0.0001	10			
Glycosaminoglycan biosynthesis – keratan sulfate	0.00031	8			
Glycosphingolipid biosynthesis – ganglio series	0.00399	7			
Biotin metabolism	0.00222	1			

the immune system and liver injury were identified as the putative target pathways in the 3 h/HAL group; however they were also identified in the 3 h/ISO group (Supplemental Tables 1 and 2). Therefore, the miRNAs specifically changed 3 h after HAL administration were not likely to participate in liver injury.

This pathway enrichment analysis could identify some biological pathways that occur in a set of miRNA target genes. However, this approach has several shortcomings because it suggests many biological pathways that are presumably affected by miRNAs, making the results difficult to interpret or validate. In addition, this method has difficulty determining which miRNAs are the most involved in a particular function's regulation.

During the next analysis, we examined whether a miRNA–mRNA pair or a targeted gene was involved in the HAL-induced liver injury; we performed an analysis using the Medical Subject Headings (MeSH) terms for the targeted gene sets of differentially expressed miRNAs, focusing on the miRNAs candidates that were involved in the early phases of HAL-induced liver injury. The genes selected by the MeSH keyword are listed in Supplemental Table 3. MeSH terms related to inflammation, immune systems and liver injury, such as "apoptosis", "cell adhesion", "glutathione", "hepatitis", "immunity, innate", "inflammation", "liver diseases", "necrosis", and "oxidative stress," were extracted from the target genes of down-regulated miRNAs in the 1 h/HAL administration group because the putative target pathways selected by KEGG pathway analysis are likely to be involved in regulation of the inflammation and immune systems, as well as liver injury. The genes reportedly targeted by miRNA (as determined by experimental evidence) were downloaded from the miRTarBase (Hsu et al., 2011) (http://mirtarbase.mbc.nctu.edu.tw/).

Supplementary material related to this article can be found, in the online version, at http://dx.doi.org/10.1016/j.tox.2014.02.011.

For further analysis, we selected the set of target gene and miRNA that associated with more than five keywords of MeSH from the targeted genes in Supplemental Table 3. Forty sets of miRNA/targeted genes are summarized in Table 6. During the continued miRNA selection, we chose miRNA-106b because its expression level was relatively high (40-Ct = 10.13) before it was substantially decreased (more than four-fold (0.17-fold)) as a

Table 6
Summary of immune-, inflammation- or hepatotoxicity-associated genes including the genes targeted by the miRNAs whose expressions were changed after HAL administration.

miRNA	40-Ct	Fold change at 1 h	Classification									Total
			Target gene	(a)	(b)	(c)	(d)	(e)	(f)	(g)	(h)	(i)	
mmu-miR-148b	5.39	0.13	Camk2a	X	X	X			X			X	5
mmu-miR-106b	10.13	0.17	**Mapk14**	X	X	X		X	X		X	X	7
mmu-miR-106b	10.13	0.17	**Stat3**	X	X	X	X	X	X	X	X	X	9
mmu-miR-21	12.79	0.22	Fasl	X	X	X	X	X	X	X	X	X	9
mmu-miR-21	12.79	0.22	Pten	X	X	X	X	X	X	X		X	8
mmu-miR-29b	8.21	0.24	Bak1	X	X			X	X	X	X	X	7
mmu-miR-29b	8.21	0.24	Bcl2 l11	X	X	X			X			X	5
mmu-miR-200c	8.41	0.25	Flt1	X	X			X	X	X	X	X	7
mmu-miR-27b	10.01	0.26	Smad3	X	X	X		X	X	X		X	7
mmu-miR-27a	10.64	0.26	Pparg	X	X				X	X		X	5
mmu-miR-200a	9.13	0.29	Ctnnb1	X	X	X		X	X	X		X	7
mmu-miR-200a	9.13	0.29	Flt1	X	X			X	X	X	X	X	7
mmu-miR-93	11.72	0.29	Stat3	X	X	X	X	X	X	X	X	X	9
mmu-miR-497	6.79	0.32	Bcl2	X	X	X		X	X	X	X	X	8
mmu-miR-30a	13.14	0.34	Bdnf	X	X	X		X	X			X	6
mmu-miR-30a	13.14	0.34	Egfr	X	X	X		X	X	X	X	X	8
mmu-miR-148a	12.29	0.34	Camk2a	X	X	X			X			X	5
mmu-miR-126-5p	15.26	0.34	Sfpi1	X	X			X	X			X	5
mmu-miR-17	15.48	0.35	Mapk14	X	X	X		X	X		X	X	7
mmu-miR-17	15.48	0.35	Stat3	X	X	X	X	X	X	X	X	X	9
mmu-miR-152	11.36	0.36	Camk2a	X	X	X			X			X	5
mmu-let-7d	12.78	0.36	Bdnf	X	X	X		X	X			X	6
mmu-miR-20b	6.13	0.40	Hif1a	X	X	X	X	X	X		X	X	8
mmu-miR-20b	6.13	0.40	Vegfa	X	X	X			X	X	X	X	7
mmu-miR-145	13.29	0.42	Irs1	X	X	X			X	X		X	6
mmu-miR-145	13.29	0.42	Klf4	X	X			X	X		X	X	6
mmu-miR-145	13.29	0.42	Prkce	X	X	X			X		X	X	6
mmu-miR-15a	8.55	0.43	Bcl2	X	X	X		X	X	X	X	X	8
mmu-miR-15a	8.55	0.43	Ccnd1	X	X	X				X	X	X	6
mmu-let-7c	11.28	0.44	Myc	X	X			X	X		X	X	6
mmu-let-7c	11.28	0.44	Sall4	X	X	X		X	X			X	6
mmu-miR-126-3p	18.18	0.44	Sfpi1	X	X			X	X			X	5
mmu-miR-24	16.38	0.44	Smad3	X	X	X		X	X	X		X	7
mmu-miR-295	7.22	0.45	Cdkn1a	X	X	X	X	X	X	X	X	X	9
mmu-miR-125b-5p	11.07	0.47	Tnf	X	X	X	X	X	X	X	X	X	9
mmu-miR-30d	11.95	0.47	Bdnf	X	X	X		X	X			X	6
mmu-miR-31	14.19	0.49	Hif1a	X	X	X	X	X	X		X	X	8
mmu-miR-31	14.19	0.49	Pdgfb	X	X			X	X		X		5
mmu-miR-101a	11.21	0.50	Akt1	X	X	X			X		X	X	6
mmu-miR-101a	11.21	0.50	Dusp1	X	X	X		X	X		X	X	7

The shading over the 40-Ct values indicates that the miRNA is relatively highly expressed in the liver (40-Ct > 10). The shading over the fold changes indicates a significant difference (fold change <0.25). The X's mean that the target gene is included in the MeSH keyword-associated gene sets. The following letters represent the MeSH keywords. (a) Apoptosis, (b) cell adhesion, (c) glutathione, (d) hepatitis, (e) immunity, innate, (f) inflammation, (g) liver diseases, (h) necrosis, and (i) oxidative stress.

member of the 1 h/HAL-administered group. In addition, MAPK14 and STAT3 were suggested to be targeted genes (Table 6).

3.4. Time-dependent changes in the expression level of hepatic miR-106b in HAL-induced liver injury

To validate the miRNA array data and the subsequent *in silico* analyses, we measured the time-dependent changes in the miR-106b expression level. The hepatic miR-106b's expression level decreased significantly 0.5 h, 12 h and 24 h after HAL administration relative to that of the vehicle-based control (Fig. 5).

3.5. Time-dependent changes in the mRNA and protein expression level of miR-106b

The two selected target genes of miR-106b (MAPK14 and STAT3) were analyzed using real-time PCR and immunoblotting. STAT3 was significantly increased in both the mRNA (Fig. 6A) and protein (Fig. 6B) levels 3 and 6 h after the HAL administration, respectively. The expression levels of MAPK14 were significantly increased at the mRNA level (Fig. 6) but were significantly decreased at the protein level (Fig. 6D); therefore, there was no correlation between these expression levels.

3.6. Activation of STAT3 in HAL-induced liver injury

We found that miR-106b was differentially down-regulated between 0.5 and 24 h after HAL administration (Fig. 5). STAT3 was significantly increased during HAL-induced liver injury (Fig. 6A and B) because it was targeted by miR-106b. Previously, we reported that IL-17 was involved in HAL-induced liver injury in mice (Kobayashi et al., 2009). IL-17 are mainly produced by Th17 cells and induce many inflammatory cytokines and chemokines, such as MIP-2; therefore, they have a key role in neutrophil infiltration (Zhu and Paul, 2008). The differentiation of the Th17 cells are regulated by STAT3 and RORγt (Ivanov et al., 2007). STAT3 is an upstream regulator of RORγt (Yang et al., 2007). Therefore, to clarify the involvement of STAT3 in HAL-induced liver injury, we studied whether STAT3 was activated by HAL administration. We found that the expression level of phosphorylated STAT3 was significantly increased 3 h after HAL administration (Fig. 7A). The mRNA expression level of RORγt increased 24 h after HAL administration (Fig. 7B). Therefore, the down-regulated miR-106b up-regulated the STAT3 expression levels during the period immediately after HAL administration; consequently, STAT3 is an important target in HAL-induced liver injury.

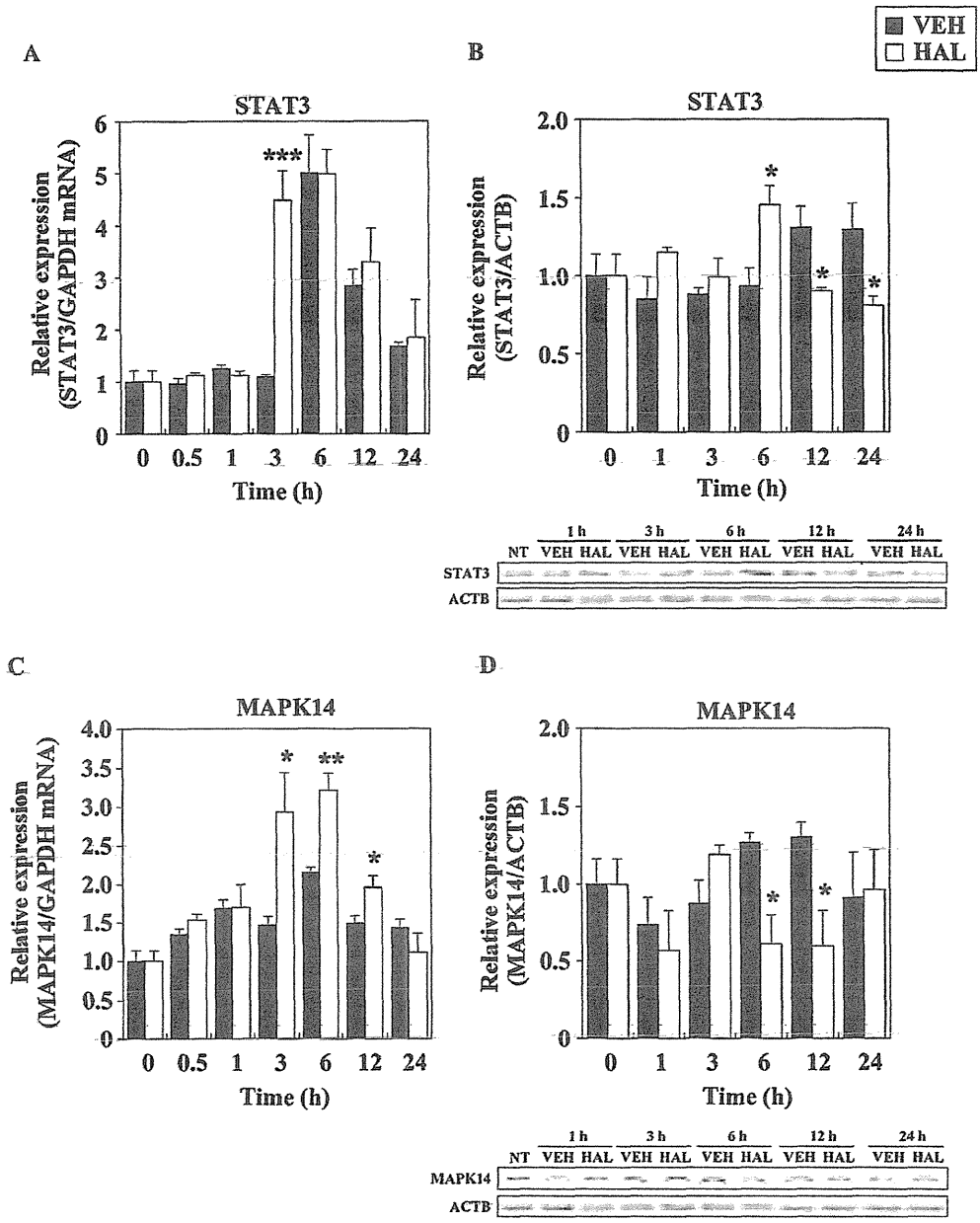

Fig. 6. Time-dependent changes in the expression of target genes, particularly in their mRNA and protein levels during HAL-induced liver injury. Mice were administered intraperitoneally with 30 mmol/kg HAL. At 0, 0.5, 1, 3, 6, 12 and 24 h after administration, the livers were collected to assess the expression levels of the hepatic mRNA and protein levels. The hepatic mRNA expression levels (A, C) were normalized to those of GAPDH. The hepatic protein expression levels (B, D) were normalized to those of ACTB. Data are represented as the means ± SEM ($n = 4$). $^{*}P < 0.05$, $^{**}P < 0.01$ and $^{***}P < 0.001$ compared to the VEH group at each time point. VEH: vehicle-treated group, HAL: halothane-treated group. ACTB: β-actin.

4. Discussion

Several reports have been published describing the effects of environmental stressors, chemicals, and drugs on miRNA expression levels (reviewed in Chenand et al., 2013; Hou et al., 2011; Lema and Cunningham, 2010; Yokoi and Nakajima, 2013). However, the exact alteration mechanisms for the miRNAs induced by xenobiotic/drug exposure remain largely unknown. In this study, approximately 30–50% of the detected miRNAs were differentially changed by more than two-fold at every different time point after HAL- administration in mice (Table 2). Hou et al., 2011 proposed that the oxidative stress and/or inflammation caused by exposure to environmental chemicals directly affected miRNAs expression. Therefore, HAL or its reactive metabolites might cause oxidative stress in the liver, directly altering the miRNA expression.

We performed comprehensive and time-dependent analysis of miRNA expression during HAL-induced liver injury in mice, revealing that the miRNAs were differentially expressed from the beginning of HAL-induced liver injury (Table 2 and Fig. 3). Additionally, ISO, low hepatotoxicity and similar structure to HAL, was used as the reference drug to exclude other pharmacological effects of halothane and to identify the specific miRNA associated with the onset of halothane-induced liver injury. Surprisingly, approximately 40% of the detected miRNAs were also differentially changed by more than two-fold at 1 and 3 h after ISO-administration in mice (Table 3). Being members of inhaled

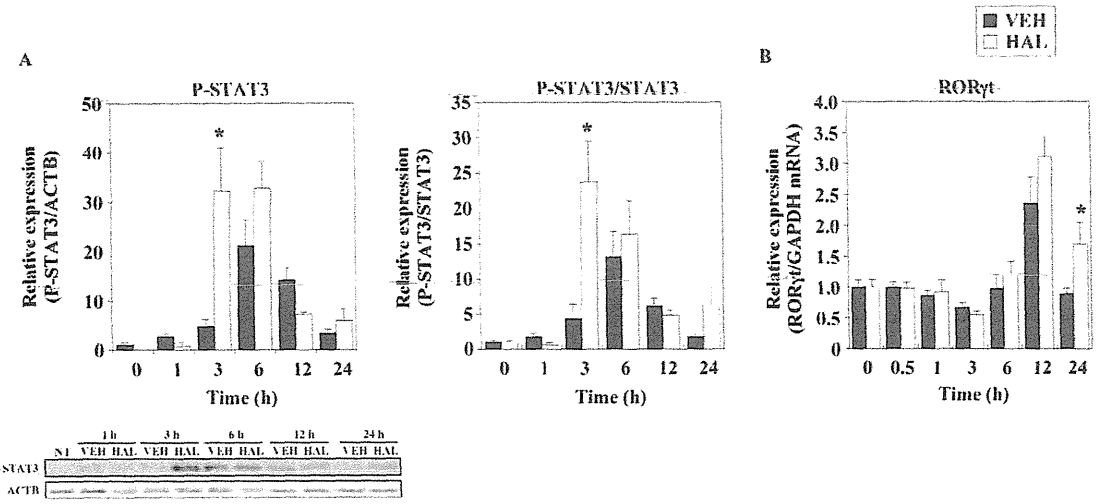

Fig. 7. Time-dependent changes in the hepatic protein (STAT3 and phosphorylated STAT3) and mRNA (RORγt) expression levels in HAL-induced liver injury. Mice were administered intraperitoneally 30 mmol/kg HAL. At 0, 1, 3, 6, 12 and 24 h after the administration, the livers were collected to assess the hepatic protein expression and mRNA levels. The STAT3 hepatic protein expression levels and phosphorylated STAT3 (A) were normalized to those of ACTB. The RORγt hepatic mRNA expression level (B) was normalized to that of GAPDH. Data are represented as the means ± SEM ($n = 4$). *$P < 0.05$ compared to the VEH group at each time point. VEH: vehicle-treated group, HAL: halothane-treated group, ACTB: β-actin.

anesthetics, HAL and ISO can produce significant effects of myocardial and respiratory depression. These effects may affect on the liver and alter the hepatic miRNA expression profiles. Therefore, we sought that specific miRNAs associated with the onset of halothane-induced liver injury may be elucidated by comparing the pathway/function of targets of miRNA altered by HAL with ISO (Fig. 4, Tables 4 and 5, and Supplemental Tables 1 and 2). *In silico* analyses revealed that the miRNAs down-regulated 1 h after HAL administration likely involved the activation of immune- or inflammation-related factors (Table 5). Moreover, we examined whether the miRNA/mRNA pairs predicted *in silico* were involved during HAL-induce liver injury; miR-106b/STAT3 was identified as a target during the early phases of HAL-induced liver injury. STAT3 is a crucial transcriptional factor for differentiating Th17 cells (Wei et al., 2007). In addition, we previously reported that HAL-induced liver injury is mediated by IL-17 in mice (Kobayashi et al., 2009). Those results validated the data obtained in the present study. In short, comprehensive miRNA expression analysis followed by *in silico* target prediction could be a new and useful approach for elucidating the miRNA–mRNA target pair involved in drug-induced liver injury.

As shown in Table 6, STAT3 and MAPK14 are genes targeted by miR-17 paralogs, such as miR-106b and miR-20a. The 3′ UTR of STAT3 and MAPK14 mRNA have a binding sequence for miR-106b; a reporter gene with this binding sequence is downregulated when miR-17 paralogs are overexpressed in a binding-sequence specific manner (Carraro et al., 2009). In addition, studies using cell lines revealed that miR-17 paralog knockdown upregulates STAT3 and MAPK14 protein expression (Carraro et al., 2009). As presented in Fig. 6A–D, the mRNA levels of STAT3 (Fig. 6A) and MAPK14 (Fig. 6C) increased significantly after HAL administration. Western blot analysis revealed that the STAT3 protein level increased significantly by HAL administration (Fig. 6B), but the MAPK14 protein level was not (Fig. 6D). This observation is not yet understood. Recently, STAT3 and MAPK14 were identified as target genes for miR-125b (Surdziel et al., 2011; Tan et al., 2012). Altering the expression levels of miRNA might affect the various signaling pathways through its targets genes because a single miRNA has multiple targets through the binding sequences, possibly explaining the results.

STAT3 mRNA and protein levels significantly increased after HAL administration (Fig. 6A and B). We previously reported that IL-17 was involved in HAL-induced liver injury (Kobayashi et al., 2009). IL-17 is primarily produced by Th17 cells and induces many inflammatory cytokines and chemokines, such as MIP-2; IL-17 also has a key role in neutrophil infiltration and activation (Zhu and Paul, 2008). The differentiation of Th17 cells is regulated by STAT3 and RORγt (Ivanov et al., 2007). Therefore, STAT3 might be important during HAL-induced liver injury. Up-regulating STAT3 using HAL induces IL-17 production, exacerbating the HAL-induced liver injury.

Many studies have been conducted to identify circulating miRNA as biomarker for DILI. Currently, miR-122 and miR-192, both are enriched in the liver, exhibited changes in the plasma that parallel serum aminotransferase levels and the histopathology of liver degeneration. Wang et al., 2009 found that the miR-122 and miR-192 expression levels decreased in the liver of acetaminophen-administered mice; these miRNA levels were increased in plasma samples. These mechanisms are thought to be leakage from liver tissue to blood, similar to the serum ALT or AST enzymes. However, in the present study, miR-106b expressed at relatively low level in the liver compared to miR-122 and miR-192. The expression level of serum miR-106b showed very low level (data not shown), thus, serum miR-106b is not likely to be a good serum biomarker for DILI.

The HAL-induced liver injury mouse model was well-established, and the mechanism of HAL-induced liver injury involves immune responses, such as neutrophil infiltration, IL-17 induction, and natural killer cell stimulation (Cheng et al., 2010; Kobayashi et al., 2009; You et al., 2006), suggesting that many immune factors facilitate the development and progression of HAL-induced liver injury. The inhibition of progesterone receptor and decrease of the immune response may have important therapeutic implications in HAL-induced liver injury (Toyoda et al., 2011). The hepatotoxic drugs, such as carbamazepine, diclofenac, dicloxacillin, flutamide, and phenytoin, as well as HAL, are known to rarely cause severe hepatotoxicity in humans. Recently, the mouse DILI models of these drugs have been established by our group (Yano et al., 2012; Higuchi et al., 2011, 2012a, 2012b; Sasaki et al., 2013). These DILI models may be beneficial for predicting the risk and the mechanisms for DILI.

In conclusion, we found that miR-106b was differentially down-regulated in HAL-induced liver injury. Among its targeted genes, STAT3 was proven to be involved in HAL-induced liver injury *via in silico* analyses. The miR-106b/STAT3 pair may be involved

in HAL-induced liver injury: HAL up-regulates STAT3 by down-regulating miR-106b, inducing liver injury in the HAL-administered mice. Moreover, miR-106b might be important while eliciting HAL-induced liver injury. The experimental approaches adopted in the present study may provide new insight into DILI mechanisms.

Funding information

This study was funded by Health and Labor Sciences Research Grants from the Ministry of Health, Labor and Welfare of Japan (H23-BIO-G001).

Conflicts of interest statement

The authors declare that they have no conflicts of interest.

Appendix A. Supplementary data

Supplementary data associated with this article can be found, in the online version, at http://dx.doi.org/10.1016/j.tox.2014.02.011

References

Bourdi, M., Amouzadeh, H.R., Rushmore, T.H., Martin, J.L., Pohl, L.R., 2001. Halothane-induced liver injury in outbred guinea pigs: role of trifluoracetylated protein adducts in animal susceptibility. Chem. Res. Toxicol. 14, 362–370.

Bi, Y., Liu, G., Yang, R., 2009. MicroRNAs: novel regulators during the immune response. J. Cell Physiol. 218, 467–472.

Carraro, G., El-Hashash, A., Guidolin, D., Tiozzo, C., Turcatel, G., Young, B.M., De Langhe, S.P., Bellusci, S., Shi, W., Parnigotto, P.P., Warburton, D., 2009. miR-17 family of microRNAs controls FGF10-mediated embryonic lung epithelial branching morphogenesis through MAPK14 and STAT3 regulation of E-Cadherin distribution. Dev. Biol. 333, 238–250.

Chenand, S., Xuan, J., Guo, L., 2013. microRNAs in drug-induced liver toxicity. In: microRNAs in Toxicology and Medicine, pp. 33–47.

Cheng, L., You, Q., Yin, H., Holt, M.P., Ju, C., 2010. Involvement of natural killer T cells in halothane-induced liver injury in mice. Biochem. Pharmacol. 80, 255–261.

Friedman, R.C., Farh, K.K., Burge, C.B., Bartel, D.P., 2009. Most mammalian mRNAs are conserved targets of microRNAs. Genome Res. 19, 92–105.

Fukushima, T., Hamada, Y., Yamada, H., Horii, I., 2007. Changes of micro-RNA expression in rat liver treated by acetaminophen or carbon tetrachloride, regulation role of micro-RNA for RNA expression. J. Toxicol. Sci. 32, 401–409.

Gut, J., Christen, U., Huwyler, J., 1993. Mechanisms of halothane toxicity: novel insights. Pharmacol. Ther. 58, 133–155.

Higuchi, S., Kobayashi, M., Yano, A., Tsuneyama, K., Fukami, T., Nakajima, M., Yokoi, T., 2012a. Involvement of Th2 cytokines in the mouse model of flutamide-induced acute liver injury. J. Appl. Toxicol. 32, 815–822.

Higuchi, S., Kobayashi, M., Yoshikawa, Y., Tsuneyama, K., Fukami, T., Nakajima, M., Yokoi, T., 2011. IL-4 mediates dicloxacillin-induced liver injury in mice. Toxicol. Lett. 200, 139–145.

Higuchi, S., Yano, A., Takai, S., Tsuneyama, K., Fukami, T., Nakajima, M., Yokoi, T., 2012b. Metabolic activation and inflammation reactions involved in carbamazepine-induced liver injury. Toxicol. Sci 130, 4–16.

Hou, L., Wang, D., Baccarelli, A., 2011. Environmental chemicals and microRNAs. Mutat. Res. 714, 105–112.

Hsu, S.D., Lin, F.M., Wu, W.Y., Liang, C., Huang, W.C., Chan, W.L., Tsai, W.T., Chen, G.Z., Lee, C.J., Chiu, C.M., Chien, C.H., Wu, M.C., Huang, C.Y., Tsou, A.P., Huang, H.D., 2011. miRTarBase: a database curates experimentally validated microRNA-target interactions. Nucleic Acids Res. 39, D163–D169.

Ivanov, I.I., Zhou, L., Littman, D.R., 2007. Transcriptional regulation of Th17 cell differentiation. Semin. Immunol. 19, 409–417.

Kanehisa, M., 2002. The KEGG database. Novartis Found Symp. 247, 91–101.

Kanehisa, M., Goto, S., Hattori, M., Aoki-Kinoshita, K.F., Itoh, M., Kawashima, S., Katayama, T., Araki, M., Hirakawa, M., 2006. From genomics to chemical genomics: new developments in KEGG. Nucleic Acids Res. 34, D354–D357.

Kobayashi, E., Kobayashi, M., Tsuneyama, K., Fukami, T., Nakajima, M., Yokoi, T., 2009. Halothane-induced liver injury is mediated by interleukin-17 in mice. Toxicol. Sci. 111, 302–310.

Komagata, S., Nakajima, M., Takagi, S., Mohri, T., Taniya, T., Yokoi, T., 2009. Human CYP24 catalyzing the inactivation of calcitriol is post-transcriptionally regulated by miR-125b. Mol. Pharmacol. 76, 702–709.

Laemmli, U.K., 1970. Cleavage of structural proteins during the assembly of the head of bacteriophage T4. Nature 227, 680–685.

Latronico, M.V., Catalucci, D., Condorelli, G., 2008. MicroRNA and cardiac pathologies. Physiol. Genom. 34, 239–242.

Lee, Y.S., Dutta, A., 2009. MicroRNAs in Cancer. Annu. Rev. Pathol. Mech. Dis. 4, 199–227.

Lema, C., Cunningham, M.J., 2010. MicroRNAs and their implications in toxicological research. Toxicol. Lett. 198, 100–105.

Mohri, T., Nakajima, M., Fukami, T., Takamiya, M., Aoki, Y., Yokoi, T., 2010. Human CYP2E1 is regulated by miR-378. Biochem. Pharmacol. 79, 1045–1052.

Nelson, K.M., Weiss, G.J., 2008. MicroRNAs and cancer: past, present, and potential future. Mol. Cancer. Ther. 7, 3655–3660.

Njoku, D., Laster, M.J., Gong, D.H., Eger 2nd, E.I., Reed, G.F., Martin, J.L., 1997. Biotransformation of halothane, enflurane, isoflurane, and desflurane to trifluoroacetylated liver proteins: association between protein acylation and hepatic injury. Anesth. Analg. 84, 173–178.

O'Connell, R.M., Rao, D.S., Chaudhuri, A.A., Baltimore, D., 2010. Physiological and pathological roles for microRNAs in the immune system. Nat. Rev. Immunol. 10, 111–122.

Pillai, R.S., 2005. MicroRNA function: multiple mechanisms for a tiny RNA? RNA 11, 1753–1761.

Pogribny, I.P., Tryndyak, V.P., Boyko, A., Rodriguez-Juarez, R., Beland, F.A., Kovalchuk, O., 2007. Induction of microRNAome deregulation in rat liver by long-term tamoxifen exposure. Mutat. Res. 619, 30–37.

Ray, D.C., Drummond, G.B., 1991. Halothane hepatitis. Br. J. Anaesth. 67, 84–99.

Roderburg, C., Urban, G.W., Bettermann, K., Vucur, M., Zimmermann, H., Schmidt, S., Janssen, J., Koppe, C., Knolle, P., Castoldi, M., Tacke, F., Trautwein, C., Luedde, T., 2011. Micro-RNA profiling reveals a role for miR-29 in human and murine liver fibrosis. Hepatology 53, 209–218.

Sasaki, E., Matsuo, K., Iida, A., Tsuneyama, K., Fukami, T., Nakajima, M., Yokoi, T., 2013. A novel mouse model for phenytoin-induced liver injury: involvement of immune-related factors and P450-mediated metabolism. Toxicol. Sci. 136, 250–263.

Surdziel, E., Cabanski, M., Dallmann, I., Lyszkiewicz, M., Krueger, A., Ganser, A., Scherr, M., Eder, M., 2011. Enforced expression of miR-125b affects myelopoiesis by targeting multiple signaling pathways. Blood 117, 4338–4348.

Takamizawa, J., Konishi, H., Yanagisawa, K., Tomida, S., Osada, H., Endoh, H., Harano, T., Yatabe, Y., Nagino, M., Nimura, Y., Mitsudomi, T., Takahashi, T., 2004. Reduced expression of the let-7 microRNAs in human lung cancers in association with shortened postoperative survival. Cancer Res. 64, 3753–3756.

Tan, G., Niu, J., Shi, Y., Ouyang, H., Wu, Z.H., 2012. NF-κB-dependent microRNA-125b up-regulation promotes cell survival by targeting p38α upon ultraviolet radiation. J. Biol. Chem. 287, 33036–33047.

Toyoda, Y., Endo, S., Tsuneyama, K., Miyashita, T., Yano, A., Fukami, T., Nakajima, M., Yokoi, T., 2011. Mechanism of exacerbative effect of progesterone on drug-induced liver injury. Toxicol. Sci. 126, 16–27.

Tsuchiya, Y., Nakajima, M., Takagi, S., Taniya, T., Yokoi, T., 2006. MicroRNA regulates the expression of human cytochrome P450 1B1. Cancer Res. 66, 9090–9098.

Vlachos, I.S., Kostoulas, N., Vergoulis, T., Georgakilas, G., Reczko, M., Maragkakis, M., Paraskevopoulou, M.D., Prionidis, K., Dalamagas, T., Hatzigeorgiou, A.G., 2012. DIANA miRPath v.2.0: investigating the combinatorial effect of microRNAs in pathways. Nucleic Acids Res. 40, W498–W504.

Wang, K., Zhang, S., Marzolf, B., Troisch, P., Brightman, A., Hu, Z., Hood, L.E., Galas, D.J., 2009. Circulating miRNAs, potential biomarkers for drug-induced liver injury. Proc. Natl. Acad. Sci. U.S.A. 106, 4402–4407.

Wei, L., Laurence, A., Elias, K.M., O'Shea, J.J., 2007. IL-21 is produced by Th17 cells and drives IL-17 production in a STAT3-dependent manner. J. Biol. Chem. 282, 34605–34610.

Wu, F., Zikusoka, M., Trindade, A., Dassopoulos, T., Harris, M.L., Bayless, T.M., Brant, S.R., Chakravarti, S., Kwon, J.H., 2008. MicroRNAs are differentially expressed in ulcerative colitis and alter expression of macrophage inflammatory peptide-2 alpha. Gastroenterology 135, 1624–1635.

Yang, X.O., Panopoulos, A.D., Nurieva, R., Chang, S.H., Wang, D., Watowich, S.S., Dong, C., 2007. STAT3 regulates cytokine-mediated generation of inflammatory helper T cells. J. Biol. Chem. 282, 9358–9363.

Yano, A., Higuchi, S., Tsuneyama, K., Fukami, T., Nakajima, M., Yokoi, T., 2012. Involvement of immune-related factors in diclofenac-induced acute liver injury in mice. Toxicology 293, 107–114.

Yokoi, T., Nakajima, M., 2013. microRNAs as mediators of drug toxicity. Ann. Rev. Pharmacol. Toxicol. 53, 377–400.

You, Q., Cheng, L., Reilly, T.P., Wegmann, D., Ju, C., 2006. Role of neutrophils in a mouse model of halothane-induced liver injury. Hepatology 44, 1421–1431.

Zamore, P.D., Haley, B., 2005. Ribo-gnome: the big world of small RNAs. Science 309, 1519–1524.

Zhu, J., Paul, W.E., 2008. CD4T cells: fates, functions, and faults. Blood 112, 1557–1569.

Biochemical Pharmacology 87 (2014) 660–667

Contents lists available at ScienceDirect

Biochemical Pharmacology

journal homepage: www.elsevier.com/locate/biochempharm

Epigenetic regulation of the tissue-specific expression of human UDP-glucuronosyltransferase (UGT) 1A10

Shingo Oda, Tatsuki Fukami, Tsuyoshi Yokoi [1], Miki Nakajima *

Drug Metabolism and Toxicology, Faculty of Pharmaceutical Sciences, Kanazawa University, Kakuma-machi, Kanazawa 920-1192, Japan

ARTICLE INFO

Article history:
Received 18 September 2013
Accepted 4 November 2013
Available online 14 November 2013

Keywords:
Epigenetics
DNA methylation
Tissue-specific regulation
UDP-glucuronosyltransferase

ABSTRACT

Human UDP-glucuronosyltransferase (UGT) 1A10 is not expressed in the liver; however, UGT1A10 is highly expressed in the intestine, contributing to presystemic first-pass metabolism. Earlier studies revealed that hepatocyte nuclear factor (HNF) 1α and Sp1, as well as an intestine-specific transcription factor, caudal type homeobox (Cdx) 2, are involved in the constitutive expression of UGT1A10. However, why UGT1A10 is not expressed in the liver, where HNF1α and Sp1 are abundantly expressed, is unknown. In this study, we sought to elucidate the mechanism, focusing on epigenetic regulation. Bisulfite sequence analysis revealed that the CpG-rich region (−264 to +117) around the *UGT1A10* promoter was hypermethylated (89%) in hepatocytes, whereas the *UGT1A10* promoter was hypomethylated (11%) in the epithelium of the small intestine. A luciferase assay revealed that the methylation of the *UGT1A10* promoter by *SssI* methylase abrogated transactivity even with overexpressed Cdx2 and HNF1α. The *UGT1A10* promoter was highly methylated (86%) in liver-derived HuH-7 cells, where UGT1A10 is not expressed. In contrast, the *UGT1A10* promoter was hardly methylated (19%) in colon-derived LS180 cells, where UGT1A10 is expressed. Treatment with 5-aza-2′-deoxycitidine (5-Aza-dC), an inhibitor of DNA methylation, resulted in an increase in UGT1A10 expression only in HuH-7 cells. Moreover, overexpression of HNF1α and Cdx2 further increased UGT1A10 expression only in the presence of 5-Aza-dC. Collectively, we found that DNA hypermethylation would interfere with the binding of HNF1α and Cdx2, resulting in the defective expression of UGT1A10 in human liver. Thus, epigenetic regulation is one of the mechanisms that determine the tissue-specific expression of UGT1A10.

1. Introduction

UDP-Glucuronosyltransferases (UGTs) catalyze the glucuronidation of a variety of endogenous and exogenous compounds. In humans, there are 19 functional UGT enzymes, which are classified into three subfamilies: UGT1A, UGT2A, and UGT2B [1]. The *UGT1A* genes, which are located on chromosome 2q37, contain multiple unique first exons and common exons 2–5 and encode nine kinds of functional UGT1A enzymes [2]. The *UGT2* genes, which are located on chromosome 4q13, encode three UGT2A and seven UGT2B functional enzymes.

Human UGT enzymes are expressed in a tissue-specific manner. Most UGTs, including UGT1A1, UGT1A3, UGT1A4, UGT1A6, UGT1A9, UGT2B4, UGT2B10 and UGT2B7, are predominantly expressed in the liver [3,4] and expressed to a lesser extent in extra-hepatic tissues. Several UGTs are preferentially expressed in extra-hepatic tissues, including the kidney, small intestine, colon, stomach, lungs, epithelium, ovaries, testis, mammary glands and prostate. In particular, UGT1A7, UGT1A8, and UGT1A10 are highly expressed in the gastrointestinal tract, excluding the liver. This expression limits the bioavailability of orally administered drugs, such as raloxifene, naloxon, and mycophenolic acid, as well as xenobiotics, such as resveratrol and quercetin [5,6]. The intestine-specific expression of UGT1A8 and UGT1A10 was explained by transcriptional regulation through an intestine-specific transcription factor, caudal type homeobox 2 (Cdx2), as well as Sp1 and hepatocyte nuclear factor (HNF) 1α [7–10]. However, why UGT1A8 and UGT1A10 are not expressed in the liver, where Sp1 and HNF1α are abundantly expressed, remains unsolved.

The purpose of this study was to clarify the underlying mechanisms of the defective expression of UGT1A10 in the liver, focusing on epigenetic regulation. Although UGT1A8 mRNA is substantially detected in intestine, the expression of UGT1A8 protein has never been proven. In contrast, UGT1A10 protein could be clearly detected in the intestine by Western blot analysis using

* Corresponding author. Tel.: +81 76 234 4407; fax: +81 76 234 4407.
E-mail address: nmiki@p.kanazawa-u.ac.jp (M. Nakajima).
[1] Present address: Department of Drug Safety Sciences, Nagoya University Graduate School of Medicine, Nagoya, Japan.

0006-2952/$ – see front matter © 2013 Elsevier Inc. All rights reserved.
http://dx.doi.org/10.1016/j.bcp.2013.11.001

an anti-UGT1A10 specific antibody that we prepared (unpublished data). This observation is the reason we focused on UGT1A10 in this study. It is generally accepted that epigenetics, including DNA methylation and histone modification, are key regulators of tissue-dependent gene expression [11,12]. We investigated whether DNA methylation and histone modification might be determinants of the tissue-specific expression of human UGT1A10.

2. Materials and methods

2.1. Chemicals and reagents

5-Aza-2′-deoxycytidine (5-Aza-dC) and trichostatin A (TSA) were purchased from Sigma–Aldrich (St. Louis, MO). Goat anti-human HNF1α polyclonal antibody (C-19), goat anti-human Cdx2 polyclonal antibody (C-20), and control rabbit and goat IgGs were purchased from Santa Cruz Biotechnology (Santa Cruz, CA). Primers were commercially synthesized at the Hokkaido System Science (Sapporo, Japan). All other chemicals and solvents were of the highest grade commercially available.

2.2. Human tissues

Human liver (a 39-year-old Japanese female) and small intestine (a 49-year-old Caucasian female) were obtained from autopsy materials that were discarded after pathological investigation. The use of the human liver and small intestine was approved by the ethics committees of Kanazawa University (Kanazawa, Japan) and Iwate Medical University (Morioka, Japan).

2.3. Cell culture

Colorectal adenocarcinoma cell lines LS180, Caco-2, HT-29, and SW480 and the hepatocellular carcinoma cell line HepG2 were obtained from the American Type Culture Collection (Manassas, VA). A hepatocellular carcinoma cell lines HuH-7 were obtained from the RIKEN BioResource Center (Ibaraki, Japan). HT-29 and SW480 cells were cultured in RPMI1640 (Nissui Pharmaceutical, Tokyo, Japan) that was supplemented with 10% fetal bovine serum (Invitrogen, Carlsbad, CA). The other cells were cultured as previously described [13].

2.4. RNA isolation and real-time reverse transcription (RT)-polymerase chain reaction (PCR)

Total RNA was isolated from cell lines using RNAiso (Takara, Otsu, Japan) according to the manufacturer's protocol. The cDNA was synthesized from the total RNA using Rever Tra Ace® (Toyobo, Osaka, Japan). The UGT1A10 mRNA levels were determined by real-time RT-PCR and normalized to glyceraldehyde-3-phosphate dehydrogenase (GAPDH) mRNA levels as described previously [3].

2.5. Genomic DNA extraction and bisulfite reaction

Genomic DNA samples were prepared from human hepatocytes (HH268, a 54-year-old Caucasian female, Tissue Transformation Technologies), whole small intestine or epithelium of the small intestine, and cell lines using a Gentra Puregene Tissue kit (Qiagen, Valencia, CA). Five hundred nanograms of genomic DNA digested with *EcoR* I was treated with bisulfite using an EZ DNA Methylation kit (Zymo Research, Orange, CA) according to the manufacturer's protocol. The DNA fragments spanning the transcription start site (TSS) of the *UGT1A10* or *UGT1A8* genes and the 5′-flanking region of *UGT1A9* were amplified by PCR using the primer pairs that are shown in Table 1. The PCR products were cloned into the pT7Blue T-Vector (Novagen, Madison, WI). Because the primer pair for the bisulfite analysis of UGT1A8 and UGT1A10 amplifies the corresponding regions of not only UGT1A8 and UGT1A10 but also UGT1A9, clones containing UGT1A9 sequence were precluded by digestion with *Mbo* II, and clones containing UGT1A8 or UGT1A10 sequences were subjected to sequence analysis. The DNA methylation status of the sequence was analyzed using the web-based tool QUMA [14].

2.6. Construction of expression plasmids and luciferase reporter plasmids

A luciferase reporter plasmid, pCpGL-basic, which completely lacks CpG dinucleotides, was kindly provided by Dr. Rehli [15]. The 5′-flanking regions of *UGT1A9* (−955 to +29) or the promoter region of *UGT1A10* (−365 to +140), which was amplified by PCR using the human liver genome as a template, was cloned into the pCpGL-basic plasmid. The products were termed UGT1A9/pCpGL

Table 1
Sequences of oligonucleotides that were used in the present study.

Oligonucleotides	5′ to 3′ sequence	Position
Bisulfite analysis of UGT1A8 and UGT1A10		
Forward	AGAGAGTATTTGGTTGGTTAAAG	−365 to −343[a]
Reverse	ACACTACCAACAACTTCCCTACC	+118 to +140[a]
Bisulfite analysis of UGT1A9		
Forward	TTTGAAGGAGGGTATTGGAGTGATG	−754 to −730
Reverse	CCAAACCCTAAAAAACCTCTAAAATAC	−540 to −514
Cloning of promoter region of UGT1A10		
Forward	CTTTGGATCCAGAGAGTATTTGGTTGGC	−365 to −347
Reverse	CCATAGATCTGCACTACCAGCAGCTTCCC	+122 to +140
Cloning of promoter region of UGT1A9		
Forward	GGCAGCTGCAGTTGATCTTTTCCCTTTAAG	−955 to −937
Reverse	CAGAGATCTGCAGCTGAGAG	+17 to +29
ChIP assay of UGT1A10		
Forward	AATGATACTCGTGTGTTATC	−135 to −116
Reverse	AGACACACACATAAAGGAAC	+76 to +95
Cloning of Cdx2		
Forward	CCGGACCCTCGCCACCATGTA	−16 to +5
Reverse	GTGGGTCACTGGGTGACGGT	+927 to +947

Nucleotides are numbered with the TSS designated as +1 in the genomic DNA sequence of UGTs and with base A in the initiation codon ATG designated as +1 in the Cdx2 cDNA sequence. The restriction sites that were used for cloning are underlined.
[a] The numbers refer to the nucleotide position of *UGT1A10*.

and UGT1A10/pCpGL, respectively. HNF4α and HNF1α expression plasmids were constructed previously [16,17]. For the construction of the Cdx2 expression plasmid, human Cdx2 cDNA was amplified by PCR using the primer pair that is shown in Table 1 and human small intestine cDNA as a template. The PCR product was subcloned into the pTARGET vector (Promega, Madison, MI). DNA sequencing analysis confirmed the nucleotide sequence.

2.7. Luciferase reporter assays

The pCpGL-basic, UGT1A9/pCpGL, and UGT1A10/pCpGL plasmids were treated with a CpG methylase *Sss*I (New England Biolabs, Beverley, MA). For the luciferase assays, HuH-7 cells were seeded onto a 24-well plate at 1×10^5 cells/well. After 24 h, 200 ng of pCpGL-basic plasmid and 300 ng each of human Cdx2, HNF1α, and HNF4α expression plasmids or pTARGET empty plasmid were transfected into the cells using Lipofectamine 2000 (Invitrogen). The cells were harvested 48 h after the transfection and lysed to measure the luciferase activity using a Dual Luciferase Reporter Assay System (Promega). The protein concentration was determined using Bradford protein assay reagent (Bio-Rad Laboratories, Hercules, CA) using γ-globulin as a standard. The relative luciferase activities were normalized to the protein content.

2.8. Chemical treatment and transfection of expression plasmid into the cells

HuH-7 or LS180 cells were seeded onto a 12-well plate at 0.5×10^5 cells/well and incubated for 24 h. For dose response experiments, the cells were treated with 0.01–10 μM 5-Aza-dC for 120 h or treated with 50–300 nM TSA for 24 h, and then subjected to RNA isolation. For the overexpression of HNF1α and Cdx2, the cells were treated with 0.1 μM 5-Aza-dC for 120 h. Sixty hours before harvesting, the cells were transiently transfected with 0.5 μg of an HNF1α and/or Cdx2 expression plasmids using the X-tremeGENE HP DNA transfection reagent (Roche Applied Science, Indianapolis, IN). The UGT1A10 mRNA levels were determined as described above.

2.9. Immunoblot analysis of HNF1α and Cdx2

Total cell homogenates (40 μg) from HuH-7 and LS180 cells that were transfected with HNF1α and Cdx2 expression plasmids were separated by 10% SDS-PAGE and transferred to an Immobilon-P transfer membrane (Millipore). The membranes were blocked with Odyssey Blocking Buffer (LI-COR Biosciences, Lincoln, NE) for 1 h and were probed with goat anti-human HNF1α or rabbit anti-human Cdx2 antibodies diluted 1:500 for 3 h followed by IRDye 680LT-labeled donkey anti-goat or goat anti-rabbit secondary antibodies diluted 1:5000 (LI-COR Biosciences) for 1 h. The membranes were then scanned using the Odyssey Infrared Imaging system (LI-COR Biosciences).

2.10. Statistical analyses

For the DNA methylation status, the statistical significance was evaluated by the Mann–Whitney *U*-test or Fisher's exact test using the web-based tool QUMA. For the mRNA expression and luciferase assay, the statistical significance was determined using unpaired, two-tailed Student's *t*-test or one-way analysis of variance (ANOVA) followed by Dunnett's test. Correlation analyses were performed by Spearman's rank method. When the *p* value was less than 0.05, the differences were considered statistically significant.

3. Results

3.1. DNA methylation status of the 5′-flanking regions of UGT1A8, UGT1A9, and UGT1A10 in human hepatocytes and small intestine

We searched the CpG dinucleotides between 300 bp upstream and 200 bp downstream of the TSS of human *UGT1A8*, *UGT1A9*, and *UGT1A10* genes (Fig. 1A). Five and 12 CpG dinucleotides were found around TSS (−365 to +140 bp) for *UGT1A8* and *UGT1A10*, whereas only two CpG dinucleotides were observed around TSS for *UGT1A9*. In the case of *UGT1A9*, there were multiple CpG dinucleotides spanning 800–600 bp upstream of the TSS. The DNA methylation status of the promoter regions of *UGT1A10* spanning −365 to +140 in the small intestine and liver was determined by bisulfite sequence analysis (Fig. 1B). Previously, when we used a whole liver tissue sample for the analysis of DNA methylation of UGT1A1, the results indicated a mixed methylation pattern derived from parenchymal and non-parenchymal cells [17]. Accordingly, we used hepatocytes in this study. As shown in Fig. 1B, 89% of CpG sites (128 of 144 CpG sites) in the promoter region of the *UGT1A10* gene were methylated in hepatocytes, whereas 51% of CpG sites (86 of 168 CpGs) were methylated in the whole small intestine. Notably, in the whole small intestine, the methylated CpG sites were biased in specific clones. It was surmised that these clones showing hypermethylation might be from the submucosa of the small intestine, where UGT enzymes are not expressed [18]. Therefore, epithelium cells that were prepared from the small intestine were used to determine the DNA methylation status of the *UGT1A10* promoter. The methylation status was found to be only 11% (18 of 168 CpG sites). Collectively, we found that the DNA methylation status of the *UGT1A10* promoter region was quite lower in the small intestine epithelium than hepatocytes ($p < 0.0001$, Mann–Whitney *U*-test).

Next, the DNA methylation status of the promoter of *UGT1A8*, which shows high sequence similarity with *UGT1A10*, was investigated (Fig. 1B). In the promoter of *UGT1A8* from hepatocytes, 79% of CpG sites (51 of 65 CpG sites) were methylated, whereas in the small intestine epithelium, 16% of CpG sites (9 of 55 CpGs) were methylated ($p = 0.0004$, Mann–Whitney *U*-test). The difference in the DNA methylation pattern of *UGT1A8* between two tissues was almost identical to that of UGT1A10. Because there is only one CpG site in the promoter of UGT1A9, we investigated the farther upstream CpG-rich region (−765 to −639 bp) for its DNA methylation status. In the 5′-flanking region of *UGT1A9* from hepatocytes, 93% of CpG sites (65 of 70 CpG sites) were methylated, and in the small intestine epithelium, 96% of CpG sites (67 of 70 CpGs) were methylated ($p = 0.34$, Mann–Whitney *U*-test). Thus, the DNA methylation status of this region would not be associated with the tissue-specific expression of UGT1A9.

3.2. Effects of DNA methylation on the transactivity of UGT1A10 and UGT1A9

To determine the effects of DNA methylation on promoter activity, luciferase assays were performed using methylated and unmethylated luciferase constructs (Fig. 2). In the case of the unmethylated UGT1A10/pCpGL construct, the overexpression of either Cdx2 ($p < 0.05$) or HNF1α ($p < 0.01$) highly increased the activity of luciferase, and the synergistic increase of the activity was observed by the coexpression of these factors ($p < 0.01$), supporting the previous study [8]. In the case of the methylated UGT1A10/pCpGL construct, the overexpression of Cdx2 and/or HNF1α did not significantly increase luciferase activities. Luciferase activities of unmethylated UGT1A10/pCpGL constructs were significantly higher than methylated constructs, indicating that DNA methylation statuses have a great impact on the

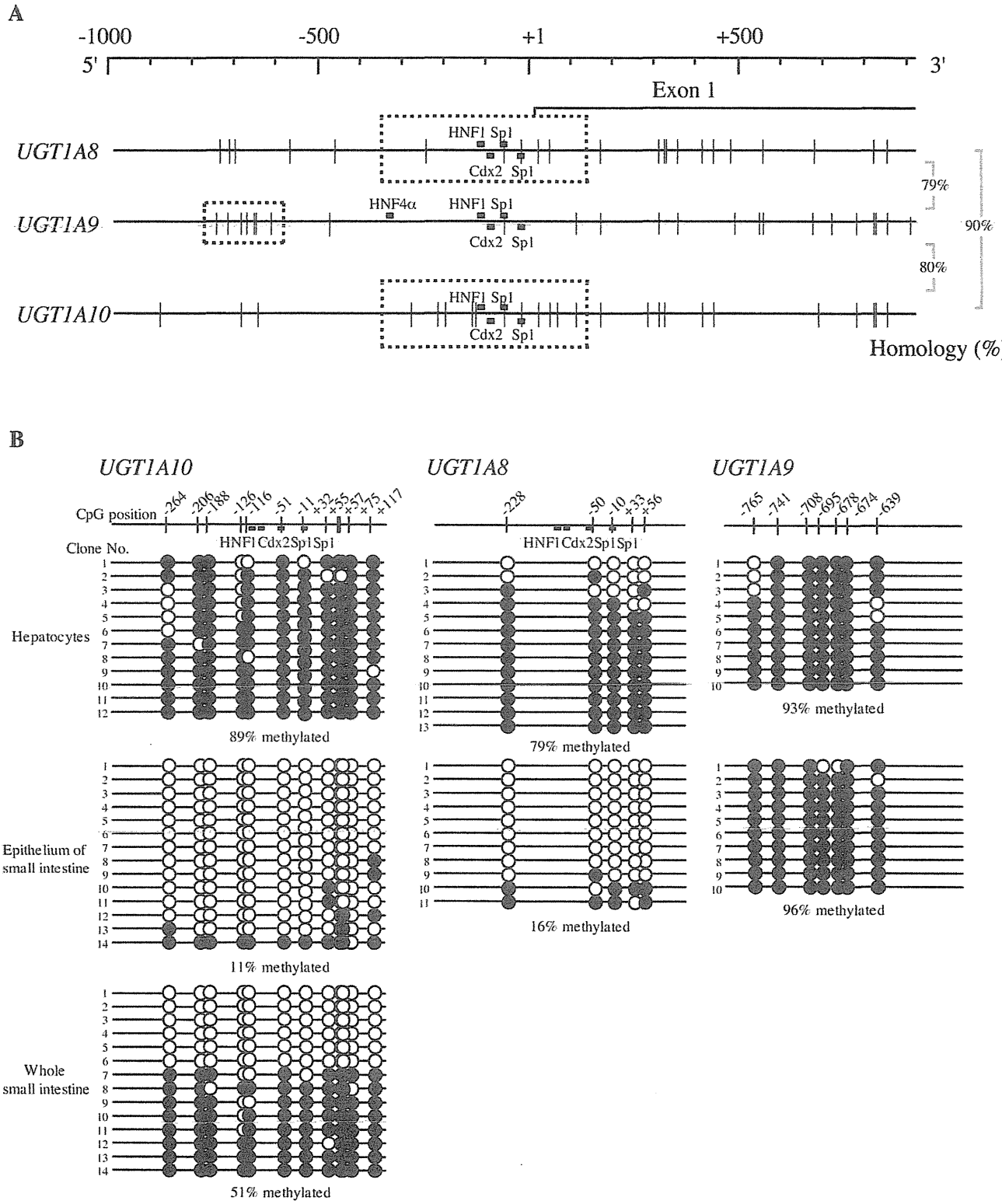

Fig. 1. DNA methylation status of *UGT1A8*, *UGT1A9*, and *UGT1A10* in human hepatocytes and small intestine. (A) A schematic diagram of the 5′-flanking region of *UGT1A8*, *UGT1A9*, and *UGT1A10*. The TSS of each UGT isoform is designated as +1. The vertical lines and rectangles represent the CpG sites and the binding sites of each transcription factor, respectively. Bisulfite sequencing was performed in the regions that are outlined with a dashed line. The homologies of −1000 bp upstream to TSS of each UGT1A isoform are shown on the right. (B) DNA methylation status of CpG sites in the 5′-flanking region of *UGT1A8*, *UGT1A9*, and *UGT1A10* genes. Bisulfite sequencing analysis was performed using genomic DNA that was extracted from human hepatocytes (HH268) or small intestine epithelium (a 49-year-old Caucasian female). For UGT1A10, the DNA methylation status in the genomic DNA that was extracted from whole small intestine was also investigated. At least ten clones from each sample were sequenced. Open and closed circles represent unmethylated and methylated cytosines, respectively.

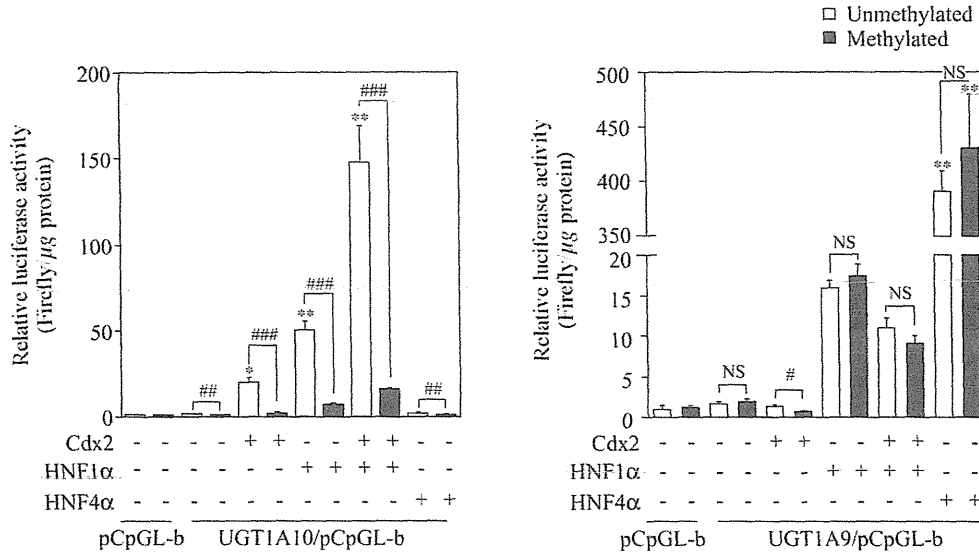

Fig. 2. Effects of DNA methylation on the transactivity of UGT1A10 and UGT1A9. pCpGL-basic plasmids containing either −365 to +140 of *UGT1A10* or −955 to +29 of *UGT1A9*, as well as pCpGL-basic plasmids, were treated with *Sss* I DNA methylase. Both the treated or untreated reporter construct and Cdx2, HNF1α or HNF4α expression plasmids were transiently transfected into HuH-7 cells. After 48 h, the cells were harvested, and the luciferase activities were measured. Each column represents the mean ± SD of relative activities (firefly/μg protein) of triplicate determinations. $^{*}p < 0.05$ and $^{**}p < 0.01$, compared with no transfection by one way ANOVA followed by Dunnett's test. $^{\#\#}p < 0.01$ and $^{\#\#\#}p < 0.001$, compared with the unmethylated construct by two-tailed Student's *t*-test.

transcriptional activity of UGT1A10. The overexpression of HNF4α did not increase the luciferase activity of UGT1A10. This observation may be because the sequence of the HNF4α recognition element in the *UGT1A10* gene was different by one nucleotide from the consensus sequence of the HNF4α response element [19]. In the case of the UGT1A9/pCpGL construct, the overexpressed HNF4α increased ($p < 0.01$) the activity regardless of methylation status, although the overexpressed Cdx2 and HNF1α did not significantly increase the activity of luciferase. These results suggest that the DNA methylation of the 5′-flanking region was not associated with the transcriptional activity of UGT1A9.

3.3. DNA methylation status of the UGT1A10 promoter region in colon- and liver-derived cell lines

We next investigated the DNA methylation status of the UGT1A10 promoter region in six kinds of human cell lines: colon adenocarcinoma cell lines, LS180, Caco2, HT29, and SW480 and hepatocellular carcinoma cell lines, HepG2 and HuH-7. The degree of DNA methylation in the *UGT1A10* promoter was, in ascending order, HT-29 < LS180 < HepG2 < SW480 < HuH-7 < Caco-2 (Fig. 3). The expression level of UGT1A10 mRNA in theses cells was measured, and the relation with the DNA methylation status was analyzed. DNA methylation levels tended to be inversely correlated with UGT1A10 mRNA expression levels (Spearman's $r = -0.54$, $p = 0.29$). These results suggest that the DNA methylation status would determine the basal expression level of UGT1A10 in cell lines. In the subsequent experiments, two cell lines, human colon adenocarcinoma LS-180 and hepatocellular carcinoma HuH-7 cells, were selected as representatives of UGT1A10-positive and -negative cells, respectively.

3.4. Effects of 5-Aza-dC and TSA on the expression of UGT1A10 mRNA

To investigate the significance of the DNA methylation at the promoter region in UGT1A10 expression, experiments using epigenetic modulatory agents were performed. When these cells were treated for 5 days with 5-Aza-dC, which is an inhibitor of DNA methylation, UGT1A10 mRNA expression was dramatically increased in HuH-7 cells (≈16-fold at maximum), whereas UGT1A10 mRNA was marginally increased in LS180 cells (≈1.6-fold at maximum) (Fig. 4A). It was confirmed that 5-Aza-dC treatment decreased the methylation status in HuH-7 cells from 86% to 60% ($p = 0.15$). Theses results demonstrated that UGT1A10 expression is silenced by DNA methylation. Unexpectedly, the methylation status in LS180 cells was slightly increased from 19% to 41% ($p = 0.09$) by 5-Aza-dC treatment, although the reason is unknown (Fig. 4B). Next, the involvement of histone acetylation for the expression of UGT1A10 was investigated. When these cells were treated for 1 day with TSA,

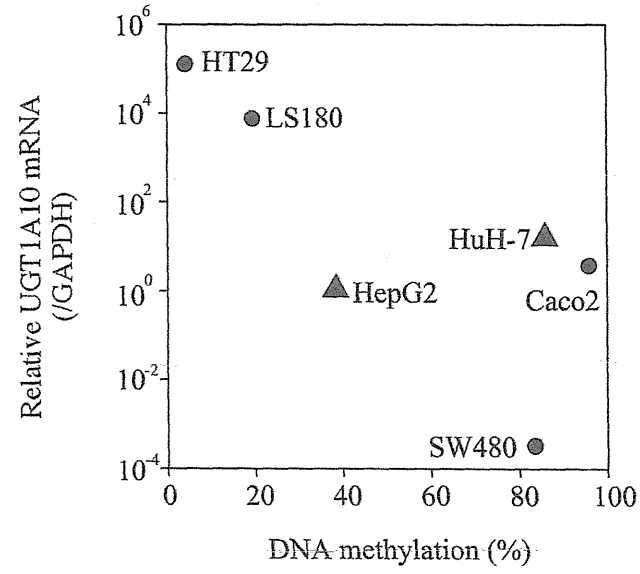

Fig. 3. Relation between the DNA methylation status of the promoter region of *UGT1A10* and mRNA expression levels of UGT1A10 in colon- (circle) and liver-derived (triangle) carcinoma cells lines. The DNA methylation status of UGT1A10 was analyzed by bisulfite sequence analysis of at least five clones for each cell. The methylation status was expressed as the percentage of methylated cytosines per total CpG dinucleotides among all of the sequenced clones. The expression levels of UGT1A10 mRNA were expressed relative to those levels in HepG2 cells.

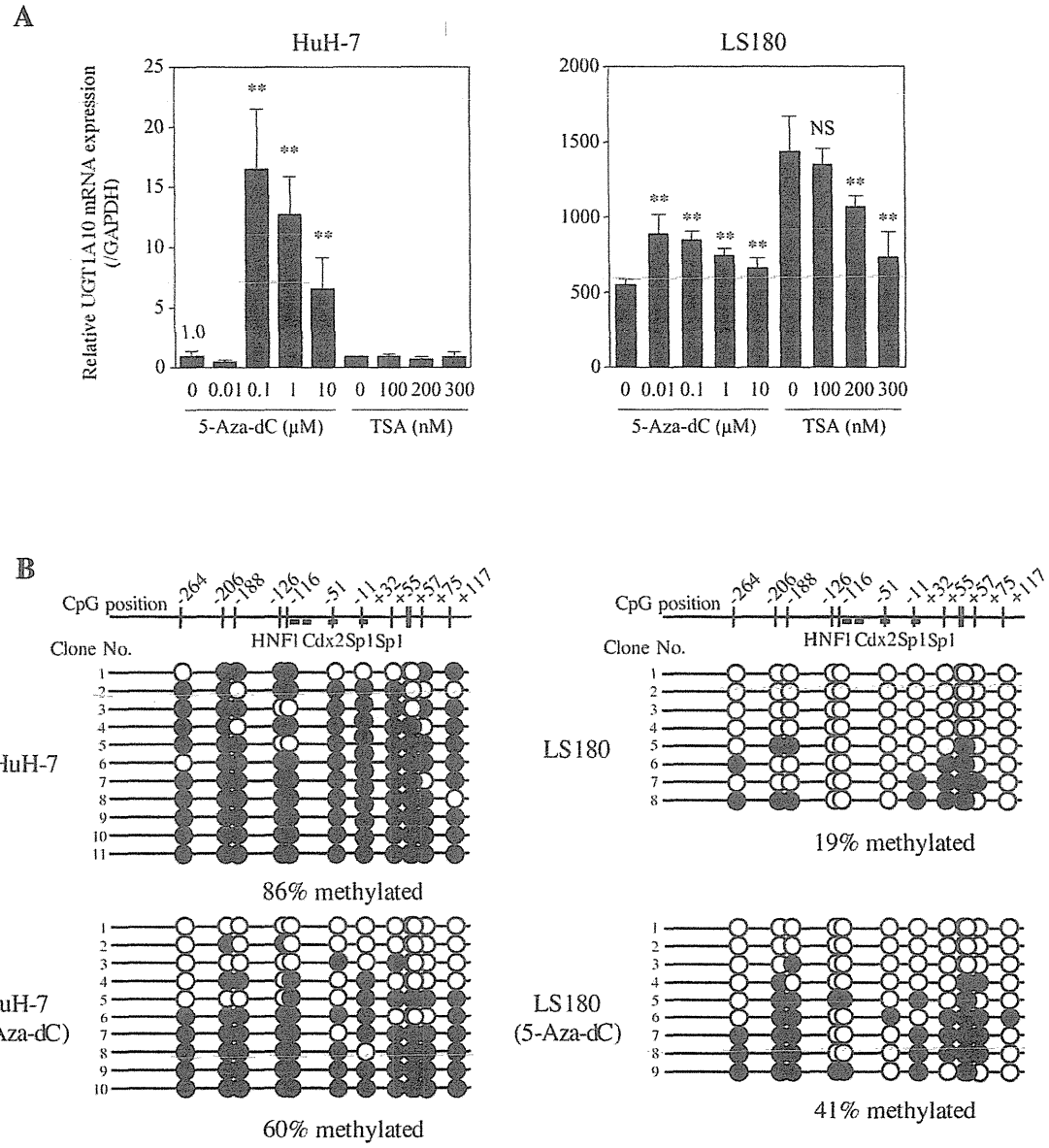

Fig. 4. Effects of 5-Aza-dC and/or TSA treatment on the UGT1A10 expression in HuH-7 and LS180 cells. (A) UGT1A10 mRNA levels in HuH-7 and LS180 cells that were treated with 5-Aza-dC or TSA, which were normalized to the GAPDH mRNA levels. Each column represents the mean ± SD of triplicate determinations. $^{**}p < 0.01$, compared with non-treated cells by one way ANOVA followed by Dunnett's test. (B) DNA methylation status of the *UGT1A10* promoter region in HuH-7 and LS180 cells before and after treatment with 0.1 μM 5-Aza-dC. Bisulfite sequencing analysis of at least eight clones for each cell was performed.

which is an inhibitor of histone deacetylase, the expression of UGT1A10 mRNA in HuH-7 cells was not changed (Fig. 4A). The expression of UGT1A10 mRNA in LS180 cells was decreased in a dose-dependent manner (Fig. 4A), but it may be due to the cytotoxicity of TSA. These results suggest that the impact of histone acetylation on the UGT1A10 regulation would be limited. The differential expression levels (≈3-fold) of UGT1A10 in LS180 cells between the controls for 5-Aza-dC and TSA treatment may be due to the difference in culture time.

3.5. Effects of 5-Aza-dC and the overexpression of HNF1α and Cdx2 on the expression of UGT1A10

We investigated whether the demethylation of DNA allows transcription factors to bind to the promoter of *UGT1A10* and thereby to activate transcription (Fig. 5). In intact HuH-7 and LS180 cells, HNF1α was marginally expressed, and Cdx2 was not expressed (Fig. 5). The transfection of HNF1α and Cdx2 expression plasmids into HuH-7 cells resulted in a dramatic increase in HNF1α and Cdx2 proteins (Fig. 5) but did not increase UGT1A10 expression (Fig. 5). However, under 5-Aza-dC treatment, the overexpression of HNF1α and Cdx2 resulted in a significant increase in UGT1A10 mRNA expression (11-fold) in HuH-7 cells. These results suggested that DNA methylation inhibits the binding of HNF1α and Cdx2 to the promoter of *UGT1A10*. The overexpression of HNF1α and Cdx2 under 5-Aza-dC treatment did not result in the upregulation of UGT1A10 in LS180 cells most likely because the extent of DNA methylation was originally low, and the endogenous HNF1α expression levels might be sufficient for the interaction with unknown components that might be essential for UGT1A10 expression in LS180 cells (Fig. 5).

4. Discussion

In this study, we investigated the underlying mechanism of defective expression of UGT1A10 in the liver focusing on

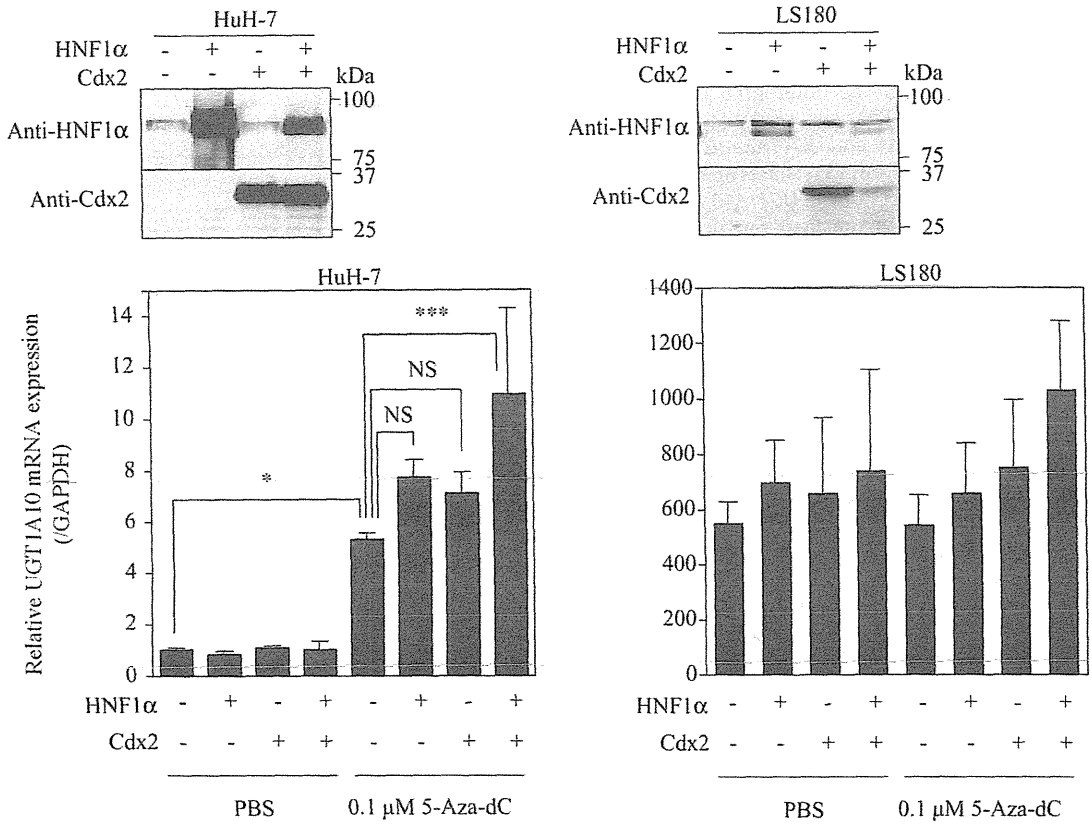

Fig. 5. Effects of 5-Aza-dC treatment and the overexpression of HNF1α and Cdx2 on UGT1A10 expression in HuH-7 and LS180 cells. The cells were treated with 5-Aza-dC followed by the transient transfection of HNF1α and/or Cdx2 expression plasmids (+) or empty plasmid (−). The expression level of UGT1A10 mRNA was determined by real-time RT-PCR and was normalized to GAPDH mRNA levels. The data were expressed relative to UGT1A10 expression compared with non-treated HuH-7 cells. The HNF1α and Cdx2 protein levels were analyzed by Western blot of total cell homogenates. Each column represents the mean ± SD of triplicate determinations. $^{*}p < 0.05$, $^{**}p < 0.01$, and $^{***}p < 0.001$, compared with non-treated cells by one way ANOVA followed by Dunnett's test.

epigenetics. We found that the CpG-rich region at the promoter of the *UGT1A10* gene was hypermethylated in the hepatocytes, whereas the CpG-rich region was hypomethylated in the small intestine epithelium (Fig. 1B). Reporter gene assays revealed that the methylation of the *UGT1A10* promoter leads to an almost complete loss of transactivity even under the overexpression of Cdx2 and HNF1α (Fig. 2). Cell line-based studies clearly demonstrated the significance of DNA methylation in the regulation of UGT1A10 as follows: (1) the substantial expression of UGT1A10 mRNA was observed in LS180 cells with the DNA hypomethylation status, (2) 5-Aza-dC treatment resulted in the increase of UGT1A10 expression, reflecting the change in the DNA methylation status, and (3) exogenously expressed HNF1α and Cdx2 could increase UGT1A10 expression only under 5-Aza-dC treatment in HuH-7 cells. These findings clearly illustrated that DNA methylation inhibits the expression of UGT1A10, and the unmethylated DNA status is a prerequisite for the transcriptional activation of UGT1A10. Concerning UGT1A8, which is also expressed in the gastrointestinal tract but not the liver, like UGT1A10, the promoter was hypomethylated in the small intestine epithelium and hypermethylated in the hepatocytes (Fig. 1B). The expression of UGT1A8 may also be regulated by DNA methylation, although this study did not examine it.

In general, gene silencing by DNA methylation is explained by following two mechanisms: (1) the methyl group physically interrupts the binding of transcription factors to their recognition sequences, and (2) methyl-CpG-binding proteins bind to the methylated DNA followed by the recruitment of corepressor molecules, including histone deacetylase, to induce chromatin structure condensation [11]. In the case of UGT1A10, the absence of CpG dinucleotides in a Cdx2 or an HNF1α recognition element unlikely to support the former mechanism although the possibility that methylated CpGs outside the elements affect the binding of these factors could not be denied. The presence of CpGs (at positions −51 and −11) in two Sp1 sites on the *UGT1A10* promoter may explain the former mechanism. The latter mechanism is also unlikely to be involved because TSA treatment to inhibit histone deacetylation did not result in the activation of UGT1A10 expression. Although we have no exclusive explanation, the other mechanisms may be involved in the DNA methylation-dependent repression of UGT1A10.

The inhibition of DNA methylation and concomitant overexpression of HNF1α and Cdx2 tremendously increased UGT1A10 mRNA levels in HuH-7 cells (Fig. 5). However, even under this condition, UGT1A10 levels remained lower than the level in intact LS180 cells (Fig. 5). This might be because the DNA methylation status in *UGT1A10* promoter of 5-Aza-dC-treated HuH-7 cells was still higher (60%) than that in intact LS180 cells (19%) (Fig. 4). Another possible reason may relate to differences in histone modifications or unidentified transcription factors that regulate UGT1A10 expression between the two cells. Sp1, which has been proven to enhance UGT1A10 promoter activity [7], was substantially expressed in both cell lines. To investigate the role of Sp1 on high expression of UGT1A10 in LS180 cells, we performed knockdown experiments using siRNA. When a siRNA for Sp1 was transfected into LS180 cells, severe cytotoxicity was observed (data not shown). The severe cytotoxicity was also observed with a siRNA for HNF1α (data not shown). This may be caused because

these transcription factors are indispensable for cell proliferation. Thus, the knockdown experiments unfortunately could not provide additional information. Further analysis is required to uncover the mechanism of the differential expression level of UGT1A10 in HuH-7 and LS180 cells.

In contrast with UGT1A10 and UGT1A8, UGT1A9, of which the promoter sequence (−1 kb from TSS) shares 80% and 79% similarity with the promoter sequences of the *UGT1A10* and *UGT1A8* genes, respectively, is expressed in the liver but not in intestines. As supported by the present study (Fig. 2), it has been reported that UGT1A9 is not transactivated by Cdx2 but is transactivated by HNF1α and HNF4α [8,19]. The present study found that the DNA methylation status at the 5′-flanking region of *UGT1A9* was almost the same between the small intestine and liver (Fig. 1) and that the methylation status did not affect the transcriptional activity (Fig. 2). The results suggest that the DNA methylation in the 5′-flanking region of *UGT1A9* is not associated with the tissue-specific expression of UGT1A9. Although the reason for the defective expression of UGT1A9 in the small intestine remains to be studied, the involvement of histone modification or repressive transcription factors may be possible.

Our previous study demonstrated that DNA hypermethylation and histone H3 hypoacetylation results in the defective expression of UGT1A1 in the kidney, revealing the impact of epigenetic modification in the tissues-specific expression of UGT1A1 [17]. In this study, we found that UGT1A10 expression is distinctly regulated by DNA methylation. Previous studies have revealed that the expression of UGT1A6, UGT2B15, and UGT2B28 [20] as well as UGT2B7 and UGT2B11 [21], in cancer cell lines were increased by treatment with 5-Aza-dC or valproate, which is also a DNA methylation inhibitor. Although the DNA methylation status of these five UGT isoforms has not been investigated, the tissue- or cell-specific expression of most UGTs may be epigenetically regulated.

Interestingly, accumulating evidence reveals that inverse correlation was observed between the extent of DNA methylation and expression levels among individuals for some gene such as CYP1A2, monoamine oxidase A, ATP-binding cassette A1, SLC6A4, and SLC22A2 [22–26]. This raises a possibility that interindividual variability of DNA methylation contributes to the variability in the UGT1A10 expression, although the present study did not investigate it because we focused on the tissue specific expression. Yasar et al. [27] reported for UGT1A1 that there was no clear inverse correlation between the DNA methylation and interindividual variability of gene expression in 46 individual livers. This may occur because they used whole liver sample, which contains non-parenchymal cells not expressing UGT1A1. It would be of interest to investigate the association between the interindividual variability of UGT expression and the extent of DNA methylation with careful selection of tissues or cell types.

In summary, we found that DNA methylation in the *UGT1A10* gene promoter limits the binding of transcription factors to repress the expression of UGT1A10 in the liver. The finding provides novel mechanisms of the tissue-specific expression of UGT1A10.

Acknowledgments

We acknowledge Drs. Yasuhiro Aoki and Masataka Takamiya of the Iwate Medical University for supplying human tissues and Dr. Michael Rheli of the University Hospital Regensburg for providing the pCpGL-basic vector.

References

[1] Mackenzie PI, Bock KW, Burchell B, Guillemette C, Ikushiro S, Iyanagi T, et al. Nomenclature update for the mammalian UDP glycosyltransferase (*UGT*) gene superfamily. Pharmacogenet Genomics 2005;15:677–85.

[2] Ritter JK, Yeatman MT, Ferreira P, Owens IS. Identification of a genetic alteration in the code for bilirubin UDP-glucuronosyltransferase in the *UGT1* gene complex of a Crigler-Najjar type I patient. J Clin Invest 1992;90:150–5.

[3] Izukawa T, Nakajima M, Fujiwara R, Yamanaka H, Fukami T, Takamiya M, et al. Quantitative analysis of UDP-glucuronosyltransferase (UGT) 1A and UGT2B expression levels in human livers. Drug Metab Dispos 2009;37:1759–68.

[4] Court MH, Zhang X, Ding X, Yee KK, Hesse LM, Finel M. Quantitative distribution of mRNAs encoding the 19 human UDP-glucuronosyltransferase enzymes in 26 adult and 3 fetal tissues. Xenobiotica 2012;42:266–77.

[5] Ritter JK. Intestinal UGTs as potential modifiers of pharmacokinetics and biological responses to drugs and xenobiotics. Expert Opin Drug Metab Toxicol 2007;3:93–107.

[6] Basu NK, Ciotti M, Hwang MS, Kole L, Mitra PS, Cho JW, et al. Differential and special properties of the major human *UGT1*-encoded gastrointestinal UDP-glucuronosyltransferases enhance potential to control chemical uptake. J Biol Chem 2004;279:1429–41.

[7] Gregory PA, Gardner-Stephen DA, Lewinsky RH, Duncliffe KN, Mackenzie PI. Cloning and characterization of the human UDP-glucuronosyltransferase *1A8*, *1A9*, and *1A10* gene promoters: differential regulation through an interior-like region. J Biol Chem 2003;278:36107–14.

[8] Gregory PA, Lewinsky RH, Gardner-Stephen DA, Mackenzie PI. Coordinate regulation of the human UDP-glucuronosyltransferase *1A8*, *1A9*, and *1A10* genes by hepatocyte nuclear factor 1alpha and the caudal-related homeodomain protein 2. Mol Pharmacol 2004;65:953–63.

[9] Gregory PA, Lewinsky RH, Gardner-Stephen DA, Mackenzie PI. Regulation of UDP glucuronosyltransferases in the gastrointestinal tract. Toxicol Appl Pharmacol 2004;199:354–63.

[10] Mackenzie PI, Hu DG, Gardner-Stephen DA. The regulation of UDP-glucuronosyltransferase genes by tissue-specific and ligand-activated transcription factors. Drug Metab Rev 2010;42:99–109.

[11] Shiota K. DNA methylation profiles of CpG islands for cellular differentiation and development in mammals. Cytogenet Genome Res 2004;105:325–34.

[12] Ohgane J, Yagi S, Shiota K. Epigenetics: the DNA methylation profile of tissue-dependent and differentially methylated regions in cells. Placenta 2008;29(Suppl. A):S29–35.

[13] Nakamura A, Nakajima M, Yamanaka H, Fujiwara R, Yokoi T. Expression of UGT1A and UGT2B mRNA in human normal tissues and various cell lines. Drug Metab Dispos 2008;36:1461–4.

[14] Kumaki Y, Oda M, Okano M. QUMA: quantification tool for methylation analysis. Nucleic Acids Res 2008;36:W170–5.

[15] Klug M, Rehli M. Functional analysis of promoter CpG methylation using a CpG-free luciferase reporter vector. Epigenetics 2006;1:127–30.

[16] Takagi S, Nakajima M, Kida K, Yamaura Y, Fukami T, Yokoi T. MicroRNAs regulate human hepatocyte nuclear factor 4α, modulating the expression of metabolic enzymes and cell cycle. J Biol Chem 2010;285:4415–22.

[17] Oda S, Fukami T, Yokoi T, Nakajima M. Epigenetic regulation is a crucial factor in the repression of UGT1A1 expression in the human kidney. Drug Metab Dispos 2013;41:1738–43.

[18] Strassburg CP, Kneip S, Topp J, Obermayer-Straub P, Barut A, Tukey RH, et al. Polymorphic gene regulation and interindividual variation of UDP-glucuronosyltransferase activity in human small intestine. J Biol Chem 2000;275:36164–71.

[19] Barbier O, Girard H, Inoue Y, Duez H, Villeneuve L, Kamiya A, et al. Hepatic expression of the *UGT1A9* gene is governed by hepatocyte nuclear factor 4α. Mol Pharmacol 2005;67:241–9.

[20] Dannenberg LO, Edenberg HJ. Epigenetics of gene expression in human hepatoma cells: expression profiling the response to inhibition of DNA methylation and histone deacetylation. BMC Genomics 2006;7:181.

[21] Valentini A, Biancolella M, Amati F, Gravina P, Miano R, Chillemi G, et al. Valproic acid induces neuroendocrine differentiation and UGT2B7 up-regulation in human prostate carcinoma cell line. Drug Metab Dispos 2007;35:968–72.

[22] Hammons GJ, Yan-Sanders Y, Jin B, Blann E, Kadlubar FF, Lyn-Cook BD. Specific site methylation in the 5′-flanking region of *CYP1A2* interindividual differences in human livers. Life Sci 2001;69:839–45.

[23] Shumay E, Logan J, Volkow ND, Fowler JS. Evidence that the methylation state of the monoamine oxidase A (*MAOA*) gene predicts brain activity of MAO A enzyme in healthy men. Epigenetics 2012;7:1151–60.

[24] Guay SP, Brisson D, Munger J, Lamarche B, Gaudet D, Bouchard L. ABCA1 gene promoter DNA methylation is associated with HDL particle profile and coronary artery disease in familial hypercholesterolemia. Epigenetics 2012;7:464–72.

[25] Sugawara H, Iwamoto K, Bundo M, Ueda J, Miyauchi T, Komori A, et al. Hypermethylation of serotonin transporter gene in bipolar disorder detected by epigenome analysis of discordant monozygotic twins. Transl Psychiatry 2011;1:e24.

[26] Saito J, Hirota T, Kikunaga N, Otsubo K, Ieiri I. Interindividual differences in placental expression of the *SLC22A2* (*OCT2*) gene: relationship to epigenetic variations in the 5′-upstream regulatory region. J Pharm Sci 2011;100:3875–83.

[27] Yasar U, Greenblatt DJ, Guillemette C, Court MH. Evidence for regulation of UDP-glucuronosyltransferase (UGT) 1A1 protein expression and activity via DNA methylation in healthy human livers. J Pharm Pharmacol 2013;65:874–83.

Toxicology Letters 224 (2014) 215–224

Contents lists available at ScienceDirect

Toxicology Letters

journal homepage: www.elsevier.com/locate/toxlet

Involvement of oxidative stress and immune- and inflammation-related factors in azathioprine-induced liver injury

Kentaro Matsuo [a], Eita Sasaki [a], Satonori Higuchi [a], Shohei Takai [a], Koichi Tsuneyama [b], Tatsuki Fukami [a], Miki Nakajima [a], Tsuyoshi Yokoi [a,*,1]

[a] Drug Metabolism and Toxicology, Faculty of Pharmaceutical Sciences, Kanazawa University, Kakuma-machi, Kanazawa 920-1192, Japan
[b] Department of Diagnostic Pathology, Graduate School of Medicine and Pharmaceutical Science for Research, University of Toyama, Sugitani, 930-0194 Toyama, Japan

HIGHLIGHTS

- We developed a mouse model of AZA-induced liver injury.
- The mechanism of AZA-induced liver injury was investigated.
- Oxidative stress is involved in AZA-induced liver injury.
- Inflammatory response contributes in the exacerbation phase of liver injury.
- Activation of the innate immune system contributes to the exacerbation phase.

ARTICLE INFO

Article history:
Received 26 August 2013
Received in revised form 23 October 2013
Accepted 23 October 2013
Available online 30 October 2013

Keywords:
Azathioprine
Oxidative stress
Inflammation
Liver injury
Model mouse

ABSTRACT

Drug-induced liver injury (DILI) is a growing concern in the fields of drug development and clinical drug therapy because numerous drugs have been linked to hepatotoxicity. However, it is difficult to predict DILI in humans due to the lack of experimental animal models. Although azathioprine (AZA), which is a widely used immunosuppressive drug, is generally well tolerated, a small number of patients prescribed AZA develop severe hepatitis. However, the mechanism underlying this process has not yet been elucidated. In this study, we developed a mouse model of AZA-induced liver injury and investigated the mechanisms responsible for the hepatotoxicity of AZA. Female BALB/c mice were orally administered AZA. After AZA administration, the plasma levels of alanine aminotransferase and aspartate aminotransferase were increased, and liver damage was confirmed through a histological evaluation. In addition, the hepatic glutathione levels and superoxide dismutase activity were significantly decreased. The plasma levels of reactive oxygen species were significantly increased during the early phase of AZA-induced liver injury, and the hepatic mRNA levels of immune- and inflammation-related factors were also significantly changed. In conclusion, oxidative stress and the subsequently activated immune- and inflammation-related factors are involved in AZA-induced liver injury.

1. Introduction

Drug-induced liver injury (DILI) is the most frequent reason for the withdrawal of a drug from the market and the cessation of new drug development by pharmaceutical companies. Due to their association with significant patient morbidity and mortality, several drugs, including bromfenac, ebrotidine, and troglitazone, have been removed from the pharmaceutical market (Holt and Ju, 2006). In most cases, the mechanisms of hepatotoxicity are unknown, and predictive experimental animal models are lacking.

Azathioprine (AZA) is an immunosuppressive drug that is often used to treat inflammatory bowel disease and autoimmune conditions, such as rheumatoid arthritis, and is often used after transplantation to avoid organ rejection (Dejaco et al., 2003; Maltzman and Koretzky, 2003; Dubinsky, 2004). However, its therapeutic potential is limited by its high incidence (15–28%) of adverse reactions, such as hepatotoxicity, bone marrow suppression, and gastrointestinal symptoms (Marinaki et al., 2004; Takatsu et al., 2009). In a prospective cohort study, the hepatotoxicity of AZA was recognized in approximately 2% of rheumatoid arthritis and psoriatic arthritis patients (Aithal, 2011). The hepatotoxicity of AZA was demonstrated *in vivo* in rats, which exhibited a less than

* Corresponding author. Tel.: +81 76 234 4407; fax: +81 76 234 4407.
E-mail addresses: tyokoi@p.kanazawa-u.ac.jp, tyokoi@kenroku.kanazawa-u.ac.jp (T. Yokoi).
[1] Present address: Department of Drug Safety Sciences Nagoya University Graduate School of Medicine 65 Tsurumai-cho, Showa-ku, Nagoya, 466-8550, Japan.

0378-4274/$ – see front matter © 2013 Published by Elsevier Ireland Ltd.
http://dx.doi.org/10.1016/j.toxlet.2013.10.025

two-fold increase in the ALT level compared with the normal level (El-Beshbishy et al., 2011; Amin and Hamza, 2005).

AZA is rapidly and almost completely converted into 6-mercaptopurine (6-MP) in the liver, and this compound is further metabolized by three enzymatic pathways (Wong et al., 2007; Hisamuddin et al., 2007). The methylation of 6-MP to the inactive 6-methyl mercaptopurine *via* thiopurine methyltransferase (TPMT) is the first pathway. The second pathway involves the metabolization of 6-MP into 6-thiouric acid, which is an inactive metabolite, by xanthine oxidase (XO). The third pathway converts 6-MP into 6-thioinosine 5-monophosphate *via* hypoxanthine guanine phosphoribosyl transferase, and this intermediate is then metabolized into active 6-thioguanine nucleotides. It has been reported that XO has the potential to generate reactive oxygen species (ROS) in human hepatocytes (Petit et al., 2008) and that the oxidation of 6-MP by XO is involved in the AZA-induced liver injury in patients with inflammatory bowel disease (Ansari et al., 2008).

In addition, AZA causes fever and rash, which suggests that inflammation-related mechanisms underlie the AZA-induced liver injury (Jeurissen et al., 1990). However, at present, the involvement of immune- and/or inflammation-related reactions in the AZA-induced liver injury has not been reported. Toll-like receptors (TLR) and the receptors for advanced glycation end products (RAGE), which are expressed on multiple innate immune cells, such as macrophages and dendritic cells, contribute to the activation of the innate immune system (Hennessy et al., 2010; Thornalley, 1998). It was recently reported that damage-associated molecular patterns (DAMPs), such as high-mobility group box 1 (HMGB1) and S100 proteins, which are the ligands of TLR and RAGE, are induced by ROS (Yao and Brownlee, 2010). The relationship between the activation of TLR4 or RAGE and DILI has been reported in acetaminophen- and carbamazepine-induced liver injury (Antoine et al., 2009; Higuchi et al., 2012b), which suggests that the pathogenesis of DILI involves the activation of the inflammatory system. However, only a few studies have investigated the mechanisms of immune- and inflammation-mediated DILI.

Cytokines and chemokines, which result in inflammation or infiltration of lymphocytes into the hepatocytes, are induced through the activation of TLR or RAGE (Lotze et al., 2007). Alternatively, cytokines are secreted by several immune cells, such as macrophages and T cells (Kita et al., 2001; Oo and Adams, 2010). Helper T (Th) cell-mediated immune responses play pivotal roles in the pathogenesis of a variety of human liver disorders (Kita et al., 2001). Th cells are subdivided into Th1, Th2, and Th17 subsets by their unique production of cytokines and characteristic transcription factors. Th1 cells require T-box expressed in T cells (T-bet) and secrete interferon (IFN)-γ. Th2 cells require the presence of GATA-binding domain (GATA)-3 and produce interleukin (IL)-4 and IL-5. Retinoid-related orphan receptor (ROR)-γt is indispensable for the differentiation of Th17 cells, which mainly secrete IL-17 (Kidd, 2003; Steinman, 2007). We previously reported the relationship between Th cell-related factors and the DILI induced by halothane (Kobayashi et al., 2009), α-naphthylisothiocyanate (Kobayashi et al., 2010), dicloxacillin (Higuchi et al., 2011), diclofenac (Yano et al., 2012), carbamazepine (Higuchi et al., 2012b), flutamide (Higuchi et al., 2012a), and methimazole (Kobayashi et al., 2012).

In this study, we established the development of AZA-induced liver injury in wild-type mice and demonstrated that oxidative stress and a set of subsequent inflammation- and immune-related factors are involved in AZA-induced liver injury.

2. Materials and methods

2.1. Chemicals

AZA was purchased from Tokyo Chemical Industry (Tokyo, Japan). Tempol was obtained from Santa Cruz Biotechnology (Santa Cruz, CA). Allopurinol was purchased from Woko Pure Chemical Industries (Osaka, Japan). Eritoran was kindly provided by Eisai Co. (Tokyo, Japan). RNAiso was purchased from Nippon Gene (Tokyo, Japan). ReverTra Ace was obtained from Toyobo (Tokyo, Japan). Random hexamer and SYBR Premix Ex Taq were obtained from Takara (Osaka, Japan). All of the primers were commercially synthesized by Hokkaido System Sciences (Sapporo, Japan). Rabbit polyclonal antibody against myeloperoxidase (MPO) was obtained from DAKO (Carpinteria, CA). The HMGB1 ELISA kit II was purchased from Sino-Test Corporation (Tokyo, Japan). The Fuji DRI-CHEM slides of GPT/ALT-PIII and GOT/AST-PIII that were used to measure the levels of alanine aminotransferase (ALT) and aspartate aminotransferase (AST), respectively, were obtained from Fujifilm (Tokyo, Japan). All of other chemicals were of either analytical grade or the highest commercially available grade.

2.2. AZA administration to mice

Female BALB/cCrSlc mice (8 weeks of age, 18–21 g) were obtained from SLC Japan (Hamamatsu, Japan). The mice were housed in a controlled environment (temperature 25 ± 1 °C, humidity 50 ± 10%, and 12-h light/12-h dark cycle) in the institutional animal facility with access to food and water *ad libitum*. The animals were acclimatized before their use in the experiments. Non-fasting mice were orally (*p.o.*) administered AZA (in corn oil) at a dose of 100, 200, and 300 mg/kg on the appropriate days. The blood and liver were collected 24 h after the last administration. A portion of each excised liver was fixed in 10% formalin neutral buffer solution. The degree of liver injury was assessed by hematoxylin–eosin (H&E) staining. The animal maintenance and treatment were conducted in accordance with the National Institutes of Health Guide for Animal Welfare of Japan, and the protocol was approved by the Institutional Animal Care and Use Committee of Kanazawa University of Japan.

2.3. GSH and GSSG levels

The mouse livers were homogenized in ice-cold 5% sulfosalicylic acid using a glass homogenizer and centrifuged at 8000 × *g* and 4 °C for 10 min. The glutathione (GSH) and glutathione disulfide (GSSG) concentrations in the supernatant were measured as described previously (Tietze, 1969).

2.4. Protein carbonyl contents and SOD activities

Protein carbonyl contents and superoxide dismutase (SOD) activities of liver homogenate were measured using a Protein Carbonyl ELISA kit (Enzo Life Science, Farmingdale, NY) and a Superoxide Dismutase Assay kit (Cayman Chemical, Ann Arbor, MI), respectively.

2.5. Administration of an antioxidant agent

The mice were intraperitoneally (*i.p.*) administered tempol, which is an antioxidant agent (200 mg/kg in PBS) at the same time as the AZA administration (200 mg/kg in corn oil, *p.o.*) during a period of five days. The plasma and liver were collected 24 h after the last AZA administration.

2.6. Administration of a xanthine oxidase inhibitor

The mice were administered allopurinol, which is a xanthine oxidase (XO) inhibitor (30 mg/kg in sterilize PBS, *i.p.*) at the same time as the AZA administration (200 mg/kg in corn oil, *p.o.*) during a period of three days. The plasma was collected 24 h after the last administration.

2.7. Hydrogen peroxide levels

The plasma hydrogen peroxide (H_2O_2) levels were measured using a Hydrogen Peroxide Assay kit (Bio Vision, Milpitas, CA).

2.8. Real-time reverse transcription (RT)-PCR

The RNA from the mouse liver was isolated using RNAiso according to the manufacturer's instructions. The expression levels of TLR2, TLR4, RAGE, S100A8, S100A9, T-bet, GATA-3, ROR-γt, IFN-γ, tumor necrosis factor (TNF)-α, IL-1β, NACHT-LRR-PYD-containing protein 3 (NALP3), and macrophage inflammatory protein (MIP)-2 were quantified by real-time RT-PCR. The primer sequences used in this study are shown in Table 1. For the RT, the total RNA (10 μg) and random hexamer (150 ng) were mixed and incubated at 70 °C for 10 min. The RNA solution was added to a reaction mixture containing 100 units of ReverTra Ace reaction buffer and 0.5 mM dNTPs in a final volume of 40 μl. The reaction mixture was incubated at 30 °C for 10 min, 42 °C for 1 h, and then 98 °C for 10 min to inactivate the enzyme. The real-time RT-PCR was performed using the Mx3000P instrument (Stratagene, La Jolla, CA). The PCR mixture contained 1 μl or 2 μl of template cDNA, SYBR Premix Ex Taq solution, and 8 pmol of the forward and reverse primers. The amplified products were monitored directly by measuring the increase in the intensity of the SYBR Green I dye (Molecular Probes, Eugene, OR).

Table 1
Sequences of primers used for real-time RT-PCR analyses.

Gene		Sequence
TLR2	FP	5′-GAA AAG ATG TCG TTC AAG GAG-3′
	RP	5′-TTG CTG AAG AGG ACT GTT ATG-3′
TLR4	FP	5′-TTC TTC TCC TGC CTG ACA CC-3′
	RP	5′-CCA TGC CAT GCC TTG TCT TC-3′
RAGE	FP	5′-GAA ACT TCT GAT TCC CGA TGG-3′
	RP	5′-GCT CAA CCA ACA GCT GAA TG-3′
S100A8	FP	5′-GAT GGC CAA CAA AGC ACC TT-3′
	RP	5′-TAG ACA TAT CCA GGG ACC CAG-3′
S100A9	FP	5′-GAT GGC CAA CAA AGC ACC TT-3′
	RP	5′-CCT CAA AGC TCA GCT GAT TG-3′
T-bet	FP	5′-CAA GTG GGT GCA GTG TGG AAA G-3′
	RP	5′-TGG AGA GAC TGC AGG ACG ATC-3′
GATA3	FP	5′-GGA GGA CTT CCC CAA GAG CA-3′
	RP	5′-CAT GCT GGA AGG GTG GTG A-3′
ROR-γt	FP	5′-ACC TCC ACT GCC AGC TGT GTG CTG TC-3′
	RP	5′-TCA TTT CTG CAC TTC TGC ATG TAG ACT GTC CC-3′
IFN-γ	FP	5′-GGC CAT CAG CAA CAT AAG C-3′
	RP	5′-TGG ACC ACT CGG ATG AGC TCA-3′
TNF-α	FP	5′-TGT CTC AGC CTC TTC TCA TTC C-3′
	RP	5′-TGA GGG TCT GGG CCA TAG AAC-3′
IL-1β	FP	5′-GTT GAC GGA CCC CAA AAG AT-3′
	RP	5′-CAC ACA CCA GCA GGT TAT CA-3′
NALP3	FP	5′-AGC CTT CCA GGA TCC TCT TC-3′
	RP	5′-CTT GGG CAG CAG TTT CTT TC-3′
MIP-2	FP	5′-AAG TTT GCC TTG ACC CTG AAG-3′
	RP	5′-ATC AGG TAC GAT CCA GGC TTC-3′
GAPDH	FP	5′-AAA TGG GGT GAG GCC GGT-3′
	RP	5′-ATT GCT GAC AAT CTT GAG TGA-3′

FP, forward primer; RP, reverse primer.

2.9. Administration of a TLR4 antagonist

The mice were intravenously (*i.v.*) treated with eritoran (50 μg/mouse in 0.2 ml of sterile saline), which is a TLR4 antagonist (Savov et al., 2005), on fifth day of the AZA administration (200 mg/kg in corn oil, *p.o.*). The blood was collected 24 h after the final administration.

2.10. Immunohistochemical staining of hepatic MPO-positive cells

The infiltration of neutrophils was assessed by immunostaining for MPO. A rabbit polyclonal antibody against MPO was used for the immunohistochemical staining of the liver as previously described by Kumada et al. (2004). Five visual fields at 400× magnification (each with an area of 0.1 mm^2) were randomly selected from each MPO-immunostained specimen, and a picture was taken with a digital camera (D-33E, OLYMPUS, Tokyo).

2.11. Statistical analysis

The data are presented as the mean ± SEM. The statistical analyses between multiple groups were performed using one-way analysis of variance (ANOVA) followed by Tukey's *post hoc* test. The comparisons between two groups were performed using two-tailed Student *t*-test. Differences with a value of $p < 0.05$ were considered statistically significant.

3. Results

3.1. Hepatotoxic effect of AZA in mice

AZA (200 mg/kg, *p.o.*) was administered to female BALB/c mice once daily for a period of six days. The plasma ALT and AST levels were significantly increased in the AZA-treated mice compared with the corn oil-treated and non-treated (NT) mice on days 3, 5, and 6 (Fig. 1A). A dose-dependent increase in the plasma ALT was observed with AZA doses of 100, 200, and 300 mg/kg, which resulted in the maximum plasma ALT levels of approximately 1900, 2500, and 2000 U/l, respectively (Fig. 1B). The repeated administration of AZA at a dose of 300 mg/kg caused high mortality (50% of the mice were dead after six days of AZA administration). We speculated that this high mortality was caused by its immunosuppressive action. A relatively high mortality was also observed after more than seven days and eight days of the administration of 200 mg/kg and a 100 mg/kg AZA, respectively. Based on these data, we selected to administer an AZA dose of 200 mg/kg once daily during a period of six days in the subsequent experiments. No increase in the ALT level was observed in the corn oil-treated mice. The time-dependent changes in hepatotoxicity after the administration of AZA for six days were investigated (Fig. 1C). Twenty-four hours after the final AZA administration, the plasma ALT level showed the maximum level. Histologically, hepatic lobular architecture was mildly distorted and swollen hepatocytes were observed here and there in AZA-treated mice (200 mg/kg for 6 days). Anisocytosis and anisonucleosis of hepatocytes reflected hepatocellular damage and regeneration. Coagulative necrosis of hepatocytes was observed occasionally (Fig. 1D). In sinusoids, lymphocytic infiltration was observed mildly.

3.2. Involvement of oxidative stress in AZA-induced liver injury

The hepatic GSH contents were significantly decreased in AZA-treated mice compared with NT mice and/or corn oil-treated mice on days 1, 3, 5, and 6. The corn oil-treated mice showed no significant change (Fig. 2A). The GSSG levels were significantly increased in AZA-treated mice compared with NT mice and corn oil-treated mice on days 3, 5, and 6. The GSH/GSSG ratio, which is used as an oxidative stress marker, exhibited a similar profile to that obtained with the GSH levels (Fig. 2A). Furthermore, other oxidative stress markers were measured. The hepatic protein carbonyl levels were significantly increased in AZA-treated mice compared with corn oil-treated mice on day 6 (Fig. 2B). SOD, which is the primary ROS detoxification enzyme, catalyze the dismutation of superoxide radicals into molecular oxygen and H_2O_2 (Fridovich, 1989). The SOD activity levels have been used as an oxidative stress marker and are significantly decreased in mice with APAP-induced liver injury (Agarwal et al., 2011). The hepatic SOD activities were significantly decreased in AZA-treated mice compared with NT mice and/or corn oil-treated mice on days 5 and 6 (Fig. 2C). The administration of the antioxidant tempol significantly decreased the plasma ALT levels, as shown by the comparison of the ALT levels in the AZA plus tempol-treated mice and the AZA-treated mice on days 4 and 5 (Fig. 2D). The significantly decreased hepatic SOD activities in the AZA-treated mice were restored by tempol treatment (Fig. 2E).

3.3. Effect of a xanthine oxidase inhibitor in AZA-induced liver injury

We investigated the effect of allopurinol, which is a xanthine oxidase inhibitor, to clarify the involvement of ROS in AZA-induced liver injury. The plasma ALT levels were significantly decreased in the AZA plus allopurinol-treated mice compared with the AZA-treated mice on day 3 (Fig. 3A). The plasma levels of H_2O_2, which is the most stable ROS, were significantly decreased 1 h after the last administration (Fig. 3B).

3.4. Involvement of receptors and ligands from the innate immune system and DAMPs in AZA-induced liver injury

To investigate whether the innate immune system is involved in AZA-induced liver injury, the mRNA expression levels of TLR2, TLR4, RAGE, S100A8, and S100A9 were measured in the liver of AZA-treated mice on days 1, 3, 5, and 6 (Fig. 4A). The mRNA

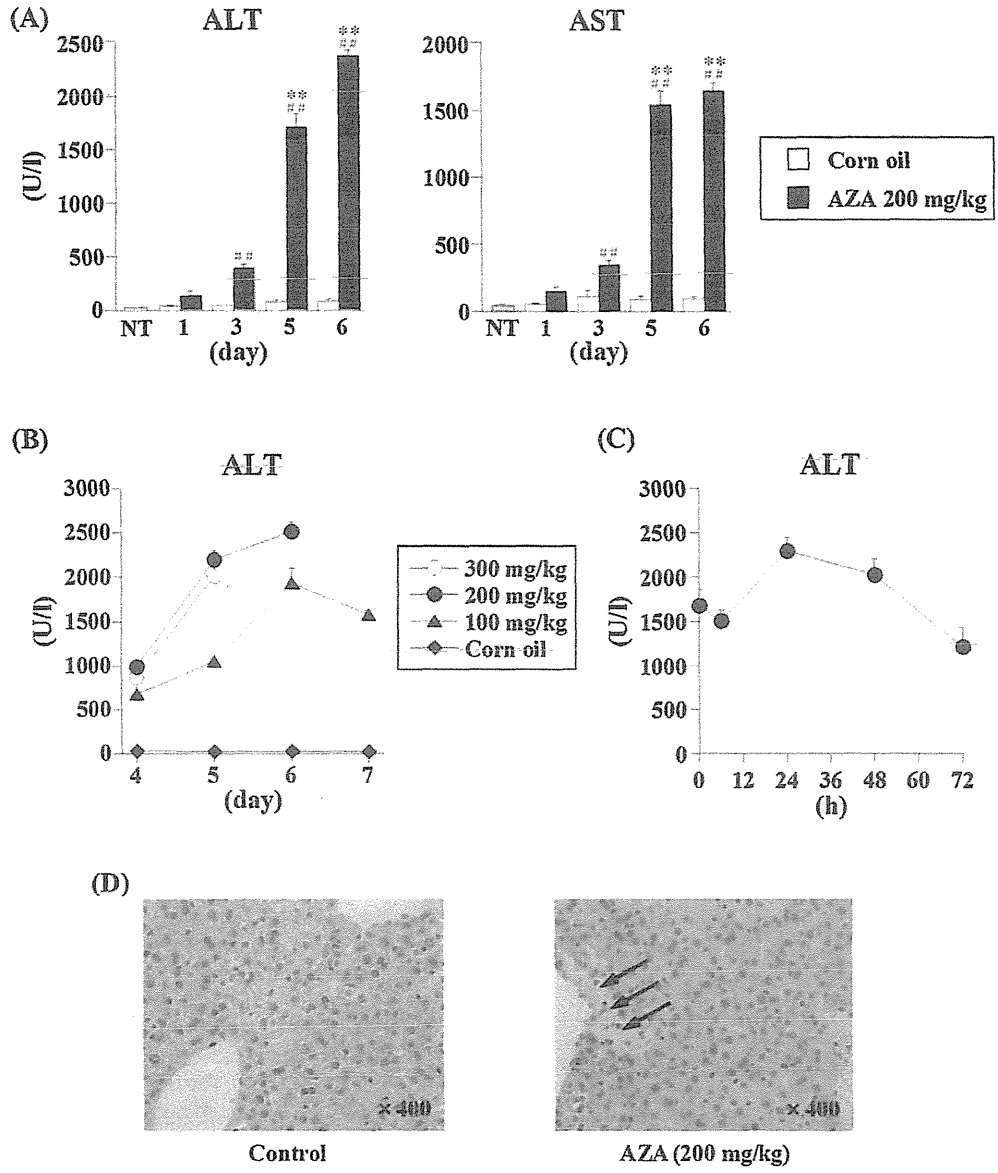

Fig. 1. Dose- and time-dependent changes in the plasma ALT and AST levels and histopathological examination of the liver of AZA-treated mice. (A) The mice were administered AZA (200 mg/kg in 10 ml/kg corn oil, *p.o.*) once daily for six days. Mice that were orally administered corn oil once daily for six days were used as the control. The plasma ALT and AST levels were measured 24 h after AZA was administered for period of one, three, five, and six days. (B) The mice were administered AZA at a dose of 100, 200, and 300 mg/kg once daily for seven, six, and five days, respectively. The plasma ALT levels were measured 24 h after AZA was administered for period of four through seven days. (C) The mice were administered AZA (200 mg/kg in corn oil, *p.o.*) once daily for six days. The plasma ALT levels were measured 0, 6, 24, 48, and 72 h after the last administration. The data represent the mean ± SEM ($n = 4$–6). **,##Significantly different compared with the non-treated (NT) mice (**$p < 0.01$) and control mice (##$p < 0.01$). (D) The liver sections from the AZA-treated mice (200 mg/kg in corn oil, *p.o.*, once daily for six days) were strained with H&E. The black arrows indicate necrotic cells.

expression level of TLR2 was significantly increased in AZA-treated mice compared with NT mice and/or corn oil-treated mice on days 3, 5, and 6. The mRNA expression level of TLR4 was significantly increased in AZA-treated mice compared with NT mice and corn oil-treated mice on days 5 and 6. The mRNA expression levels of RAGE, S100A8, and S100A9 were significantly increased in AZA-treated mice compared with NT mice and/or corn oil-treated mice on day 5. The HMGB1 protein is secreted from activated immune cells and is also passively released from necrotic cells (Wang et al., 2004). The release of HMGB1 protein is not correlated with the increased expression of hepatic HMGB1 mRNA. Thus, the plasma concentration of HMGB1 protein was measured using ELISA, and the results showed a significant increase in the amount of HMGB1 protein in AZA-treated mice compared with NT mice and corn oil-treated mice on day 6 (Fig. 4B). To investigate whether the TLR4 signaling cascade is involved in AZA-induced liver injury, mice were administered eritoran, a TLR4 antagonist, on day 5. The plasma ALT levels were significantly decreased in the AZA plus eritoran-treated mice compared with the AZA-treated mice (Fig. 4C).

3.5. Expression of T cell transcription factors and involvement of the inflammatory response in AZA-induced liver injury

To investigate the involvement of Th cells and the inflammatory response in AZA-induced liver injury, we measured the hepatic mRNA levels of immune-related transcription factors (T-bet, GATA-3, and ROR-γt) and inflammatory-related factors (INF-γ, TNF-α, IL-1β, NAPL3, and MIP-2; Fig. 5A). The mRNA expression levels

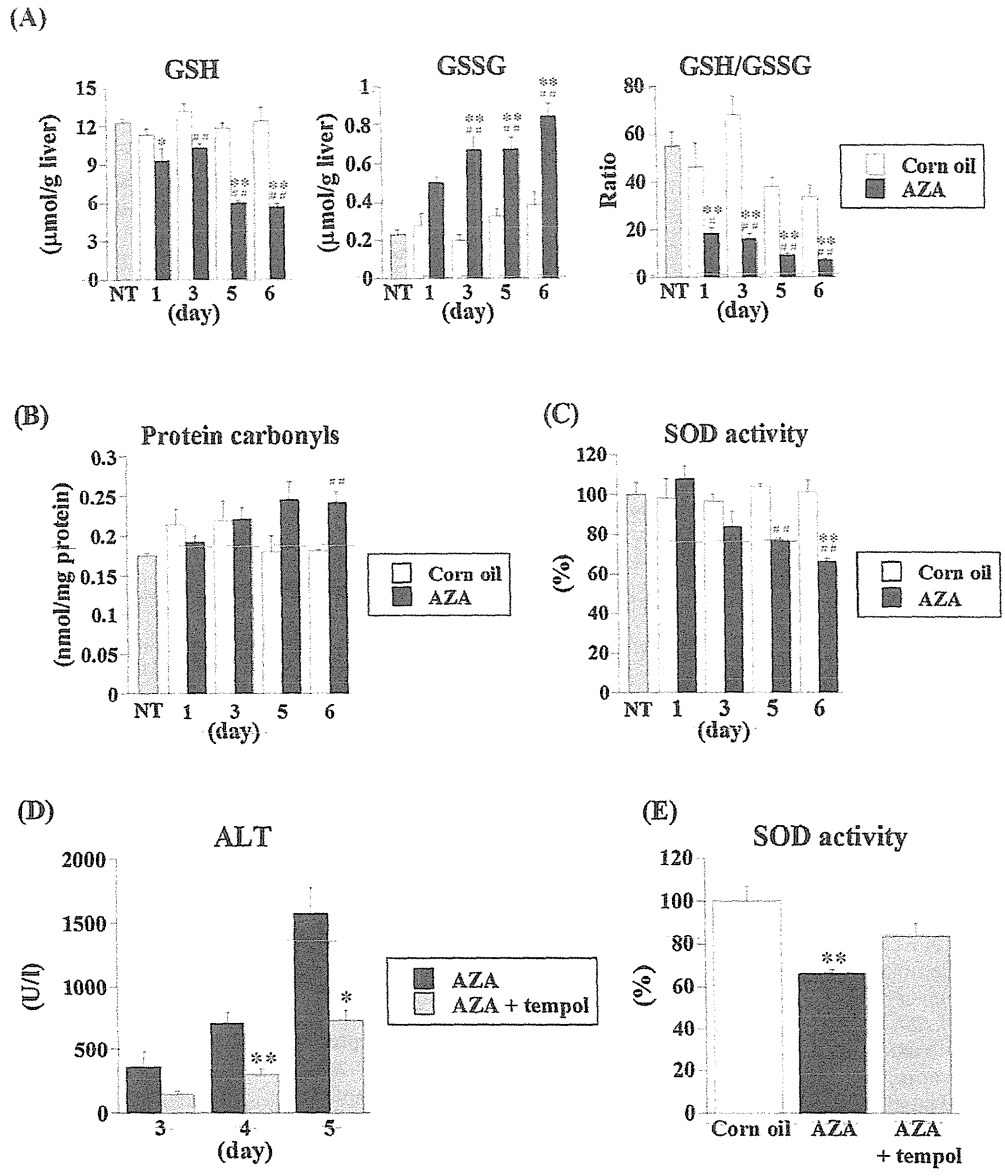

Fig. 2. Time-dependent changes in the hepatic GSH and GSSG levels and the GSH/GSSG ratio, the effect of antioxidants, and the oxidative stress marker levels in AZA-induced liver injury. The mice were administered AZA (200 mg/kg in corn oil, *p.o.*) once daily for six days. Mice that were orally administered corn oil were used as the control. The hepatic GSH and GSSG levels and the GSH/GSSG ratio (A), protein carbonyls (B), and SOD activities (C) were measured 24 h after AZA was administered for period of 1, 3, 5, and 6 days. The data represent the mean ± SEM ($n = 4$–6). *,**,#,##Significantly different compared with the non-treated (NT) mice (*$p < 0.05$, **$p < 0.01$) and control mice (#$p < 0.05$, ##$p < 0.01$). (D) The mice were administered tempol (200 mg/kg in sterilize PBS, *i.p.*) and AZA (200 mg/kg in corn oil, *p.o.*) simultaneously for a period of up to five days. The plasma ALT levels were measured 24 h after AZA was administered for three, four, and five days. The data represent the mean ± SEM ($n = 4$–6). *,**Significantly different compared with the AZA-treated mice (*$p < 0.05$, **$p < 0.01$). (E) The mice were administered tempol (200 mg/kg in sterilize PBS, *i.p.*) and/or AZA (200 mg/kg in corn oil, *p.o.*) simultaneously for five days. The hepatic SOD activities were measured 24 h after the last administration. The data represent the mean ± SEM ($n = 4$–6). **Significantly different compared with the corn oil-treated mice (**$p < 0.01$).

of TNF-α, IL-1β, and MIP-2 were significantly increased in AZA-treated mice compared with NT mice and/or corn oil-treated mice on days 5 and 6. The mRNA expression levels of T-bet and NALP3 were significantly increased in AZA-treated mice compared with NT mice and/or corn oil-treated mice on day 5. However, the expression levels of GATA-3, ROR-γt, and INF-γ were not significantly altered. Neutrophils were detected by anti-MPO antibody in immunohistochemistry. Small aggregation of neutrophils was observed here and there in hepatic parenchyma of AZA-treated mice (200 mg/kg for 6 days), while it was not observed in the corn oil-treated mice (Fig. 5B).

4. Discussion

AZA is reported to cause various adverse reactions and leads to liver injury in a small number of patients who are prescribed AZA (Marinaki et al., 2004; Takatsu et al., 2009). The mechanisms of AZA-induced liver injury have not been adequately clarified. The hepatotoxicity of AZA (less than two-fold higher than the normal level of ALT) in rats has been reported to be protected by green tea polyphenols (El-Beshbishy et al., 2011) and herbal plants (Amin and Hamza, 2005). In addition, extra-hepatic manifestations, such as fever and rash, have been reported in patients with